To the Graduate Council:

I am submitting herewith a dissertation written by Jared T. Fern entitled "Methods for the Self-Consistent Determination of Thermophysical Properties from Two-Phase Molecular Dynamics Simulations." I have examined the final electronic copy of this dissertation for form and content and recommend that it be accepted in partial fulfillment of the requirements for the degree of Doctor of Philosophy, with a major in Chemical Engineering.

David Keffer

_____

Major Professor

We have read this thesis
and recommend its acceptance:

William Steele

_____

Brian Edwards

_____

Robert Compton

_____

Carolyn R. Hodges

_____

Vice Provost and Dean of the Graduate School

(Original signatures are on file with official student records)

Methods for the Self-Consistent Determination of Thermophysical Properties from Two-Phase Molecular Dynamics Simulations

A Dissertation
Presented for the
Doctor of Philosophy
Degree
The University of Tennessee, Knoxville

Jared T. Fern
December 2007

DEDICATION

I wish to dedicate this dissertation to my wife Jennifer and to my parents Tom and Gail. Without your continued support, I would have not been able to complete this work.

ACKNOWLEDGEMENTS

I wish to acknowledge my advisors, Dr. Bill Steele and Dr. David Keffer, for your continued advice and guidance. I also wish to thank my committee members Dr. Brian Edwards and Dr. Robert Compton. There are many people that have given me guidance over the years and I cannot forget to acknowledge them: Ed Hicks, Chunggi Baig, Tudor Ionescu, Jun Mo Kim, Bangwu Jiang, Joe Lake, Mike Bleakley, and Drew Herron.

ABSTRACT

There are many tools available to measure the thermophysical properties of compounds. Experimental measurements have been evolving for many years and are very accurate at determining the properties of most compounds. However, many of the measurements are unreliable when the compound of interest is thermally unstable.

Throughout the years molecular simulation techniques have been developed to understand the thermophysical properties of thermally unstable compounds. There are primarily two methods to study Vapor-Liquid Equilibrium by molecular simulation Gibbs Ensemble Monte Carlo and Molecular Dynamics. MD is a technique that allows one to simulate the vapor and the liquid in the same simulation cell. The advantage to having the vapor and liquid in the same simulation cell is that an interface forms and properties not available by GEMC can be investigated. However, the inclusion of the interface complicates the determination of the phase densities.

There are two methods available in the literature to determine the phase densities from a two-phase MD simulation. The first utilizes a hyperbolic tangent function to fit the density profile across the axis normal to the interface. The second method calculates the average of a local property spatially and then determines the resulting distribution function. The distribution function is used to determine the phases from user defined phase cut-offs. These methods only work well far from the critical point and have many adjustable parameters. These adjustable parameters make it difficult to reliably obtain accurate results.

This lack of reliability is one of the main driving forces behind this dissertation. In order to correct the limitations of previous methods, a new technique is presented and tested against three cases. The new technique utilizes Voronoi tessellations to calculate the volume of every molecule in the simulation cell. The molecular volumes generated can be interpreted by simple statistical parameters such as the mean and variance to determine the density on the two phase envelope.

In this dissertation a new method is presented and applied to three test cases, a simple fluid, and two polyatomic cases.

TABLE OF CONTENTS

LIST OF TABLES

Table ..... Page

LIST OF FIGURES

Figure..... Page

CHAPTER 1

Introduction

Since the seminal work of van der Waals[1], the study of vapor-liquid equilibria (VLE) has generated great interest from chemical engineers. The physical properties associated with VLE (such as the critical temperature, critical density, critical pressure, coexisting vapor and liquid density, vapor pressure, and enthalpy of vaporization) are used to generate equations of state that describe how a compound will behave at a given thermodynamic state point. This information is of extreme importance to the chemical industry because many separation processes are designed around these properties.

The experimental generation of the critical properties has a long history, and ranges in complexity from visually inspecting the sample and waiting to see the critical opalescence of the system to measuring acoustic waves[2] that are generated as the system changes from two-phases to one. An example method to measure the coexisting densities, critical temperature, and critical density of a single compound is the Differential Scanning Calorimetery (DSC) method of Steele and Chirco[3]. The DSC method utilizes the calorimeter to inspect the visible changes of the system from two-phases to one. Points on the phase diagram are determined by heating a sample at a set rate and monitoring the change in energy (and heat capacity) as the temperature changes. When the sample changes from two-phases (vapor and liquid) to one (vapor), there is a change in the energy required to heat the sample. As the sample approaches the phase transition, the energy oscillates and finally spikes at the phase transition temperature. This spike corresponds to the change in heat capacity as the system changes from two-phases (liquid and vapor) to one (vapor). This process is repeated for different densities and can accurately determine the phase envelope for a compound.

Although the experimental measurements that are available are extremely precise, there are many compounds for which the critical properties cannot be determined. These compounds are thermally unstable or the equipment cannot handle the extreme temperature or pressure required to determine accurately the physical properties. For example, the thermophysical properties of ethanediol are extremely hard to measure due to thermal instability and the extreme temperature and pressures required to obtain the results accurately. The difficulty in the experimental measurements for this compound can also be seen in the quantity of disagreement in the experimental measurements available. For example, the National Institute of Standards and Technology (NIST) [4] reports five different values of the critical temperature of ethanediol spanning a 150 Kelvin range.

The difficulty in obtaining the thermophysical properties for cases such as ethanediol has led to the development of methods to predict these properties. These methods include group contribution methods, molecular based equation of states, and molecular simulation techniques[5,6]. The first two methods try to obtain the properties by using the molecular structures and summing up the contributions of each independent group within the molecule.

The use of molecular simulation to determine thermophysical properties has been evolving since the 1970's when Chapela *et al.* [7] and Ladd and Woodcock[8] first simulated a vapor and liquid in equilibrium by Molecular Dynamics (MD). The density of each phase was determined by fitting an empirical hyperbolic tangent function along the axis normal to the interface. This method of fitting was plagued with problems. The

movement of the center of mass affected the results, the phase densities could only be determined if there was a planar interface present, and the fit was not valid near the critical temperature. The fit was not valid near the critical temperature because the vapor and liquid densities are the same at the critical point, and as the system approaches the critical temperature the bulk phases break into smaller sub regions and the fit cannot account for the local regions of high and low density.

This technique was considered the state of the art until the late 1980's when Gibbs Ensemble Monte Carlo (GEMC) was developed[6,9]. One of the large problems/benefits with measuring phase equilibria with MD is the inclusion of the interface in the two-phase simulations. GEMC removed this problem by simulating the liquid and vapor phases independently. The simulation volumes are allowed to swap particles and change volumes to maintain a constant chemical potential between the two-phases. This procedure allows one to predict accurately the phase densities, the vapor pressure, and the enthalpy of vaporization within one simulation.

GEMC is widely used to this day, but also has problems. To predict accurately the phase densities, the properties at the interface were neglected. This method does not allow for one to investigate the surface tension or the molecular orientation at the interface. Furthermore, this method fails once the system starts to approach the critical temperature because the independent simulation volumes begin to swap identities[6]. To rectify this problem, additional indirect simulation methods such as Histogram Rewighting[6,9] were developed to determine the phases. Other general problems with GEMC include: difficult applications to dense systems due to low probability of

insertion, and investigation of large systems can be problematic because of the difficulty in performing calculations on parallel computers.

To address the limitations of GEMC and to include the interface, methods to investigate phase equilibrium by MD began to appear again in the literature between 2000 and today[10-12]. These methods summarized different ways to create a two-phase system within an MD simulation and created methods to extract the phase densities without the empirical hyperbolic function mentioned above.

The methods to create a two-phase system when performing MD are as follows: place a slab of liquid in contact with a slab of vapor[7], quench a vapor phase simulation[10], or expand a liquid droplet[12]. Of the three methods, the simplest to implement is the placing of a slab of vapor in contact with a slab of liquid because the location and size of the phases can be controlled. The other methods require less information for implementation, but when two-phase simulations are performed with MD many parameters have to be controlled to insure that the correct data can be extracted. These parameters include the final width of the individual phases which has to be larger than twice the interaction potential cut-off in all three directions, there has to be enough molecules in each phase to obtain good statistics, and the extent of the quench or expansion has to be such that two-phases still remain after equilibration. The quantity of molecules within each phase is controlled simply by a lever rule (a mass balance stating that the sum of the material across phases in the system is constant). If the total simulation box is too small to contain two-phases, only one phase will be present. These are just two examples of how to obtain a two-phase simulation for MD; the much larger

(and more difficult) problem is how to determine the phases within a two-phase simulation volume.

In the determination of liquid and vapor densities in a two-phase simulation, one must ultimately assign each molecule in the system to a phase. Gelb and Müller[10] developed a method for the determination of phase densities that allowed for the center-of-mass to move within the simulation volume and allowed for systems to be investigated slightly closer to the critical temperature. The method of Gelb and Müller split the simulation volume into boxes and calculated a local property such as the coordination number or the density. The local property was then expressed as an inverted histogram giving the distribution of the local property. The inverted histogram was then interpreted throughout the simulation by determining the maximum values above and below the system average and applied cut-offs to determine the density of each phase. This method was a massive leap forward because it determined the individual phase densities throughout the simulation from a local property, and corrected many of the problems associated with the hyperbolic tangent function.

However, the method of Gelb and Müller has several shortcomings. First and foremost, the definition of the limits, e.g. coordination number, used to distinguish between phases is an independent (and arbitrary) input. The VLE data obtained from this method is a strong function of these input limits. Second, the use of bins presents statistical problems when creating a probability distribution of a local property. One would like to have as many bins as possible to obtain the best statistical representation, but in the limit of very small bins, the resulting density distribution is either 1 or 0

because the bin is either occupied or unoccupied; this presents no useful information regarding the densities of the phases. The other extreme is that in the use of very large bins, the resulting density profile is that of the total system, which provides no useful information on the phase equilibrium. So, the hope is that there exists an intermediate sized bin from which the best data possible can be extracted. The optimal bin size, if it exists at all, is probably functions of thermodynamic state. This problem associated with bins makes the extraction of reliable data from two-phase MD fraught with effects due to arbitrarily chosen bin size.

The deficiencies in the all of these methods create a quagmire of adjustable parameters, empirical fits, and special case methods for the determination of phase equilibria by molecular simulation. The purpose of this dissertation is to create an improved method to determine the coexisting densities from a two-phase MD simulation. The method has to be free of arbitrary parameters, has to be self-consistent, and has to be able to determine the phases arbitrarily close to the critical point. The lack of arbitrary parameters allows for unknown systems to be investigated, because the method does not have to be calibrated. The self-consistency gives an exact parameter limit to determine the phases. To simulate arbitrary close to the critical point is a concept that cannot be achieved by any other method to date in the literature.

1.1 Summary of Work Performed

In chapter 2, two existing histogram methods are applied to determine the phase densities. A comparison of the computational burden required to obtain a two-phase system in a MD simulation is shown. The first method involves a temperature quench method and the second a volume expansion method into an unstable region in the two-phase envelope resulting in phase separation. For the comparison, methane was simulated as a Lennard-Jones fluid.

In chapter 3 a new algorithm, called the Voronoi method, is presented that allows for the determination of bulk liquid and vapor densities from a two-phase MD simulation[13]. This new method does not use any arbitrary cut-offs for phase definitions; rather it uses an iterative loop of single-phase simulations as a self-consistency check. The method does not use any spatial bins for generating histograms of local properties, thereby avoiding the statistical issues associated with bins. Finally, it allows one to approach very close to the critical point.

The new method utilizes Voronoi tessellations[14-16] to determine the molecular volume of every point at every instant in a molecular dynamics simulation. Since the molecular volume is calculated throughout the simulation, statistical parameters such as the average molecular volume and average molecular variance are easy to obtain. In order to define the phases, the normalized variance of the molecular volume from single-phase MD and two-phase MD is used as a self-consistency check. The new method gives new insight into the nature of the near sub-critical fluid. It is observed that well below

the critical temperature, some particles are neither liquid nor vapor. These interfacial particles are primarily, but not exclusively, concentrated at the bulk interface. However, as the system approaches the critical point, some particles are considered as both liquid and vapor. These interfacial particles are distributed throughout the system.

Chapter 4 is a polyatomic case study with explicit atom simulations of ethanol[17]. Simulations were performed by molecular dynamics using the OPLS-AA potential[18] and the Spherically Truncated Charge Neutralized (STCN) potential[19] for the electrostatic interactions. The phase densities were determined self-consistently by utilizing the Voronoi method presented in chapter 3. This is the first demonstration of the use of Voronoi tessellation in two-phase molecular dynamics simulation of polyatomic fluids. Properties from the two-phase simulations include: critical temperature, critical density, critical pressure, phase diagram, surface tension, and molecular orientation at the interface. The simulations were performed from 375 K to 472 K. The vapor pressure and hydrogen bonding along the two-phase envelope were also investigated. The phase envelope agreed extremely well with literature values from GEMC[20] at lower temperatures. The combined use of two-phase molecular dynamics simulation and Voronoi tessellation allows us to extend the phase diagram toward the critical point.

Chapter 5 is a second polyatomic case study. In this study ethanediol, is modeled utilizing the Transferable Potentials for Phase Equilibria (TraPPE). Simulations were performed for temperatures from 500 K to 750K. The TraPPE potential was modified to include bond stretching parameters. The parameters were determined from density functional calculations utilizing Gaussian 98[21]. The Voronoi Method[13] was used to

determine the phase densities. The resulting phase densities are approximately 9% higher on the liquid side and 26% lower on the vapor side of the phase envelope than the reported values from GEMC (these percentages are average values for available temperatures). Other properties investigated were the critical properties, surface tension, the vapor pressure, and hydrogen bonding along the phase envelope.

In Chapter 6, a summary of the work performed is provided, the implementations of this work are outlined, and several future extensions of this work are provided.

CHAPTER 2

Available Methods

Abstract
A comparison of two methods to study Vapor-Liquid Equilibrium by molecular dynamics (MD) simulation was conducted. The first method involves a temperature quench and the second a volume expansion into an unstable region in the two-phase envelope resulting in phase separation. For the comparison, methane was simulated as a Lennard-Jones fluid, using published parameters. Using a modified inverted histogram technique to solve for the liquid and vapor densities, we confirm that both techniques yield results for the densities, vapor pressure and enthalpy of vaporization in good agreement with the Lennard-Jones Equation of State and experimental data. The resulting critical properties from both methods are also obtained. The computational effort necessary to equilibrate the bulk densities is investigated as a function of simulation method and temperature. We find that the volume expansion method always equilibrates the system faster than the temperature quench method.

2.1 Introduction

The methods of measuring critical properties have been evolving for hundreds of years. The most common method is to measure the Vapor-Liquid Equilibrium (VLE) of a species. There are many different techniques available for the study of Vapor-Liquid Equilibrium (VLE). Aside from experimental measurements, computational methods have been evolving since the mid 1970's. Computational methods are a powerful tool to investigate the properties of compounds that experimental measurements cannot be conducted accurately. Ladd and Woodcock[8] first simulated phase equilibria by simulating the triple point of a Lennard-Jones fluid. This work was followed by Chapela *et al.*[7] ,who simulated a slab a liquid and a slab of vapor in contact to find the surface tension and the equilibrium densities by Molecular Dynamics.

Along with these examples for molecular dynamics simulations, there are many additional ways to simulate VLE. One common method to study phase equilibrium is by

Gibbs Ensemble Monte Carlo[6]. Other extensions of the Monte Carlo methodology are: histogram reweighting, NPT + test particle method, and the Gibbs-Duhem integration, all of which are reviewed in depth by Panagiotopoulos[9]. Another way to determine the phase equilibrium of a pure species is to use a molecularly equation of state, such as the SAFT-VXR[22].

There are known deficiencies with the Monte Carlo methods, as described by Gelb and Müller[10]. Equilibration is difficult to achieve when simulating dense phases because of the poor statistics associated with the insertion/deletion steps. Furthermore, Monte Carlo methods are difficult to apply to systems containing very complex molecules without substantial modifications, and are also difficult to implement on parallel computers.

Simulating VLE with MD in the canonical ensemble overcomes all three of these limitations since there is no particle insertion or deletion. In addition, complex fluids are routinely handled and MD codes are particularly amenable to parallelization. Perhaps more importantly, by simulating the interface, MD simulations allow for the investigation of interfacial properties such as molecule orientation, diffusion of molecules through the interface, and thickness of the interface. Furthermore, one can observe the dynamics of interface formation in MD simulations. The molecular dynamics simulations can be easily extended for use in investigating the triple point of a species where as Monte Carlo cannot. In the last few years, there have been two different methods developed to study VLE with MD. These two methods are Temperature Quench Molecular Dynamics (TQMD) and Volume Expansion Molecular Dynamics (VEMD). Both of these methods

have been compared to Monte Carlo style simulations, and the results are of comparable accuracy.

Temperature Quench Molecular Dynamics, as implemented by Gelb and Müller [10], allowed the simulation of the liquid and vapor phases in the same simulation cell. The system is equilibrated at a temperature above the critical temperature and density; then suddenly cooled to a region of mechanical and thermodynamic instability. The system then separates into liquid and vapor phases separated by an interface.

Volume Expansion Molecular Dynamics, used by Pamies *et al.* [12], also allowed for the simulation of the vapor and liquid phases to be simulated in the same cell. This method is analogous to a piston experiment where a volume of liquid is suddenly expanded to give liquid and vapor phases. The VEMD model starts as an equilibrated liquid; then the simulation cell is suddenly expanded to give a density in the unstable region along the line of rectilinear diameter. The system then separates into vapor and liquid phases separated by an interface.

Recently, a thorough comparison of TQMD, VEMD, and GEMC was published [11]. In this work, Martínez-Veracoechea and Müller simulated the VLE and VLLE of pure and binary Lennard-Jones fluids and the VLE of pure eicosane. The simulations attempted to obtain values for the liquid and vapor densities before the planar interface had formed. They found the methods to be equivalent and report obtaining density values within their prescribed tolerance for TQMD within fewer steps than VEMD.

In this chapter, a new comparison between TQMD and VEMD for the VLE of a pure Lennard-Jones fluid is made. A modified algorithm to locate the liquid, gas, and

interfacial regions is also presented. The simulation results are compared with an analytical equation of state [23] and with experimental data for methane [24,25]. The resulting critical properties are reported. The transient behavior of the interface formation during equilibration of the simulation was investigated, and the time constants associated with this process for both methods are shown as functions of temperature. A method for determining the enthalpy of vaporization and the resulting data is reported (see Figure 2.1[*]). Contrary to the earlier report [11], it is found that VEMD equilibrates faster than TQMD at all temperatures for the case that was investigated herein.

A second purpose of this chapter is to evaluate how well simulated VLE data compares to experimental VLE data, when no attempt is made to fit the parameters to existing VLE data. This is an important issue for the simulation of VLE of materials for which experimental data is not available.

2.2 Molecular Simulation Technique

In this work, molecular dynamics simulations were conducted on Lennard-Jones methane in the canonical (N,V,T) ensemble, using an in-house designed, rigorously tested FORTRAN 90 with MPI code. The Nosé-Hoover thermostat [26,27], which has been proven to generate trajectories in the canonical ensemble, is used to maintain temperature. The equations of motion were integrated using the fifth-order Gear Predictor-Corrector algorithm[5,28,29] with a time step of 2 fs. Standard periodic boundary

[*] All figures and tables appear in the appendices

conditions and minimum image convention were used. For both the VEMD and TQMD simulations, 8000 particles were simulated. The Lennard-Jones parameters were $\sigma = 3.78$ Å, $\varepsilon = 154$ K [30]. For the simulations a cut-off distance of 5σ was used, as recommended by Gelb and Müller[10]. This large cut-off is required since it is not possible to use the traditional long-range correction factor to the energy and pressure due to the inhomogeneous nature of the system. Considerable attention has previously been given to the choice of cut-off distance[31,32].

The VEMD simulation was carried out essentially as described by Pamies *et al*[12], although differences in the identification of the interface will be discussed shortly. The simulation was initially performed in a cubic cell (aspect ratio 1:1:1) at the temperature of interest and a liquid density outside the two-phase envelope. After a preliminary equilibration of 10 ps, the simulation box was instantly expanded to an aspect ratio of 1:1:2.5. The system was then allowed to equilibrate for 2 ns, which will be shown to be much longer than necessary at low and intermediate temperatures. Results for the vapor and liquid density were then collected for 2ns.

The TQMD simulation was essentially carried out as described by Gelb and Müller[10], and differences in the identification of the interface will be discussed shortly. A volume (aspect ratio of 1:1:2.5) was simulated at a temperature above the critical temperature (220 K) and at a density approximately along the line of rectilinear diameter. The choice of the volume shape imposes a preferential orientation of the interface. After a preliminary equilibration of 10 ps, the set point of the Nosé-Hoover thermostat was instantly changed. The system was then equilibrated for 2 ns, and results were collected

for 2 ns. The presence of the Nosé-Hoover thermostat is intended as a small perturbation to the Hamiltonian and resulting symplectic equations of motion, but the large temperature quench is not a perturbation and the resulting dynamics of the system may diverge from the canonical ensemble during the quench step. During equilibration only, the TQMD simulations contained a thermostat control loop to speed up the decrease in temperature. This loop works by increasing the Nosé-Hoover frequency while the simulation temperature was 60 K or greater than the set temperature. The large frequency was 8×10^{-4} fs^{-1} and the standard value used otherwise (and in data production) was 1×10^{-4} fs^{-1}. All reported mean values and standard deviations of the properties were generated using block averages, where each block was of duration 0.4 ns.

2.2.1 Method of Determining Liquid and Vapor Densities and Interface Regions

The method of calculating the densities of the liquid and vapor phases differed in some ways from previous algorithms. A one-dimensional histogram of density was generated along the long axis of the simulated volume. At each sampling point, the histogram was inverted to give a distribution function of densities among the bins. The two maxima (one necessarily below and one necessarily above the bulk density) in the density distribution were then located. Once the maximum in the density distribution corresponding to the liquid phase was found, an average liquid density was calculated by integrating over the density distribution from a set lower limit to infinity. (In other words, any density distribution above the liquid maximum was considered as a liquid.)

The lower limit of integration was determined by identifying as liquid any bins immediately beneath the maximum, with a probability at least 50% of the maximum peak value. This was included to account for the possibility that our discrete distribution might split the density peak.

The gas phase was identified in an analogous manner, using the peak in the density distribution below the average density. The lower limit of integration was zero. The upper limit of integration for the vapor phase was determined in the same way that the lower limit of integration for the liquid phase was chosen. These integrations were performed at every sampling point, so that we are able to report mean values and standard deviations based on these instantaneous values. See Figure 2.2 for an illustration of this method.

This method is insensitive to the number of bins in the histogram of density as functions of position at low temperatures. However, far too few (e.g., 3) or far too many (e.g., approaching the number of molecules) bins will produce meaningless results. In this study, 21 bins were used for the histogram of the density as functions of space. Far from the critical point, this choice places the entire interfacial region in one or two bins, so that there is over 90% of the molecule contributing to the calculation of liquid or vapor densities. Finally, 100 bins were used for the density distribution, and the density spanned the range from zero to 10 times the average density.

This method of identifying the liquid and vapor phases differs from that of Gelb and Müller [10] in several ways. First they used a three-dimensional histogram. Second, they used coordination number rather than density as their determination of liquid, gas or

interfacial phase. Third, they used an arbitrary cut-off of 30% in their coordination number.

The method also differs from that of Pamies *et al.*[12]. Pamies *et al.* found the density profile along the z axis with respect to the center of mass of the system, and did not report an algorithm for the location of the interfacial particles. The density profile was then shown as functions of the z axis (the longest axis).

2.2.2 Method of Vapor Pressure and Enthalpy of Vaporization

As shown in Figure 2.1, we performed three simulations at each temperature. The first simulation is the two-phase NVT simulation as described above. The key information obtained from this simulation is the density of the liquid and vapor phases. For reasons discussed below, to calculate the vapor pressure, a second single-phase vapor simulation was performed at the vapor density along the phase envelope. The key outputs from the vapor simulation are the vapor pressure and the vapor enthalpy. A third simulation is then performed in which we have only the liquid phase in the NpT ensemble, at the vapor pressure and temperature of interest. The key output from the liquid simulation is the liquid enthalpy, used to calculate the enthalpy of vaporization. This procedure is completely rigorous and minimized errors associated with the estimation of the vapor pressure, liquid density, and enthalpies from the inhomogeneous, two-phase simulation.

2.3 Results and Discussion

The densities of the equilibrated phases were obtained by integrating the appropriate portions of the distribution function of density. This histogram expresses the frequency of a given density value at a particular system configuration. It can then be averaged over the course of the simulation. Figure 2.3 shows the density distribution function for some of the VEMD simulations as functions of temperature.

Far from the critical point, see two very clear peaks in the distribution corresponding to the liquid and vapor phases are can be seen. As the temperature increases, the peaks move closer and the occupancy of the range of densities between the two peaks increases. Just below the critical point, one can see that there are two peaks that still correspond to liquid and vapor densities, using this algorithm. This is in contrast to Gelb and Müller[10], who did not obtain coexisting densities above T = 184.8 K. One temperature above the critical temperature is shown to indicate that the method now generates a density distribution with a single peak.

2.3.1 Thermodynamic Properties

As described above, the instantaneous density distribution was integrated resulting in instantaneous liquid and vapor densities, which were then averaged over time. The resulting phase envelope is shown in Figure 2.4 for both VEMD and TQMD simulations. Also shown in Figure 2.4 is the phase envelope from the Lennard-Jones

equation of state (LJEOS)[23] and experimental data[25]. The agreement of the simulation data with the equation of state and the experimental data for methane as functions of reduced temperature is excellent.

The average error of the liquid phase density between the VEMD simulations and the LJEOS is 0.6%. The average error of the liquid phase density between the VEMD simulations and the experimental data[25] is 1.7%. The average error of the liquid phase density between the TQMD simulations and the LJEOS is 4.5%, and between the TQMD simulations and the experimental data is 2.6%. As for the vapor phase densities, the average error between the VEMD simulations and the LJEOS is 8.1% and between the VEMD simulations and the experimental data is 11.4%. For the vapor phase densities, the average error between the TQMD simulations and the LJEOS is 9.2%, and between the TQMD simulations and the experimental data is 14.5%. All of these errors are reported with respect to the experimental reduced properties, for example, temperature/critical temperature. The densities obtained from the simulations are shown in Table 2.1. The uncertainties are one standard deviation from the simulation data collected during data production.

The vapor pressure of the two-phase simulation was not calculated because the typical expression for the pressure includes a long-range correction to the virial, which assumes a homogeneous system. While there are techniques to obtain the pressure in an inhomogeneous system[33], a different but rigorous approach is chosen to determine the vapor pressure. (One should note that the methods used to calculate the pressure in an inhomogeneous system are also used to find the interfacial properties such as the surface

tension. In this work, surface tension is not reported because the focus of this work is on the vapor and liquid densities, vapor pressure, enthalpy of vaporization, and critical properties.) Once the vapor density was obtained from the two-phase simulation, a single-phase simulation of the vapor phase was performed in the NVT ensemble at the vapor density. From the single-phase simulation, the vapor pressure and enthalpy of the vapor phase were determined. The values for the pressure and enthalpy included the long range corrections for the pressure and energy. This approach sacrifices some computational efficiency in exchange for rigorous physical properties. The resulting vapor pressures are compared to the vapor pressures predicted by the LJEOS[23]and to experimental data[25] in Figure 2.5.

The average relative error of the vapor pressure between the VEMD simulations and the LJEOS is 3.0%, and the average relative error between the VEMD simulations and experimental data is 12.4%. The largest deviations of the vapor pressure as compared to experimental data were at low values of reduced temperature due to the small values obtained.

It should be mentioned that if one were to repeat the vapor pressure calculation using the liquid phase densities generated by the VEMD simulations, one obtains a poor estimate of the vapor pressure. This is due, rather obviously, to the fact that $\left(\frac{\partial p}{\partial V}\right)_{T,N}$ is huge in the liquid phase. Thus a small error in the density induces a significant error in the pressure. In fact, for low temperatures, this frequently resulted in negative vapor pressures.

The critical properties from the VEMD and TQMD simulation results were estimated by fitting the density data to the following equations:

$$\Delta\rho = B\left(T_c - T\right)^{\beta} \quad (1)$$

$$\overline{\rho} = \rho_c + A\left(T - T_c\right) \quad (2)$$

The critical temperature was found by fitting the simulation data for the difference in the liquid and vapor densities to equation (1)[34]. For VEMD, the parameters are B = 86.94 and $\beta = 0.3458$. The resulting critical temperature is T_c =197.6K ± 0.4K. The values for the critical density were found from equation (2)[35] using the critical temperature determined from equation 1. The parameters for equation 2 are A = -0.6365 and the resulting critical density is ρ_c = 149.5 kg/m^3 ± 0.2 kg/m^3. The reported errors represent one standard deviation of the data. The TQMD model was fit to the same set of equations to give a critical temperature of T_c =197.5K ± 0.8K and a critical density of ρ_c = 157.9 kg/m^3 ± 0.4 kg/m^3 The LJEOS has a critical temperature of $T_c = 1.316\varepsilon$ (202.7 K) and a critical density of ρ_c = 0.304 molecules/Å^3 (149.5 kg/m^3). The resulting errors for the critical density and temperature versus the LJEOS are 2.4% and 0.3% respectively for the VEMD model, and the errors for the TQMD model are 2.5% for the critical temperature and 5.3% for the critical density. The errors of the critical temperature and density when compared to experimental data[25] for methane are 3.7% and 8.0% respectively for the VEMD model. The errors for the TQMD model when compared to experimental data for methane are 3.6% for the critical temperature and 2.6% for the critical density.

The critical pressure was determined by fitting the simulated vapor pressure data to the Antoine Equation shown in equation (3)[34]. The resulting critical pressure is 46.0

bar ± 0.4 bar and the resulting error for the critical pressure is 11% compared to the LJEOS and 0.1% when compared to experiment.

2.3.2 Dynamics of Interface Formation

As can be seen in Table 2.1, both the TQMD and the VEMD methods obtain the same values for the density within error. The defining difference between them is the time necessary to reach an equilibrated density of the liquid and vapor phases. As noted above, a recent report observes a faster equilibration for TQMD than for VEMD[11], which seems counter-intuitive. Figures 2.6a and 2.6b show the liquid and vapor densities for both VEMD and TQMD simulations as functions of time from the moment of quench or expansion at temperatures of (a) 123 K and (b) 189 K.

Despite the fact that some of these curves have local features, the data was fit to simple exponentials, from which we computed the corresponding relaxation times, in order to obtain a characteristic time scale of the interface formation. The relaxation times are given in Table 2.2.

From Figure 2.7 one can see that for both VEMD and TQMD the relaxation time increases with increasing temperature. This is because as the temperature increases to the critical temperature the length of time necessary to form a stable interface increases. Figure 2.7 also shows that the VEMD method equilibrates faster than the TQMD method at all temperatures.

It is conjectured that the TQMD model takes longer to equilibrate because as the temperature cools the interface has to determine its orientation within the simulation cell. In order to insure a planar interface in the z direction, the simulation geometry of a rectangle was chosen with z being the long dimension. The interface forms normal to this direction because it is the only way to minimize the surface area of the interface. This is not an issue with the VEMD model because the planar interface has the correct orientation immediately upon expansion. It is also conjectured that unreported differences in the simulation details could lead to these differing results regarding the relative efficiency of VEMD and TQMD methods. For example, the difference may be affected by the value of the frequency of the Nosé-Hoover thermostat. Again, we used 8.0×10^{-4} fs^{-1} for the quench step and 1.0×10^{-4} fs^{-1} for the equilibrated temperature and production steps of the simulation. Martínez-Veracoechea and Müller[11] did not report the value used for the thermostat frequency. However, as noted above, there is some physical significance to the relaxation times associated with interface formation due to the VEMD technique, since it mimics a macroscopic piston experiment. While the TQMD technique is intended to mimic a macroscopic temperature quench, it is unclear that the Nosé-Hoover thermostat will generate trajectories in the canonical ensemble when the system temperature is far from the set temperature. As a result, there is an uncertainty associated with the relaxation times of the TQMD method.

2.3.3 Enthalpy of Vaporization

The enthalpy of vaporization was determined by using the definition of the enthalpy, H = U + pV. The procedure to calculate this quantity is shown in Figure 2.1 and involved three simulations at each temperature. The vapor phase density was calculated from the two-phase NVT simulation. A single-phase NVT simulation was performed at the vapor phase density, generating the vapor pressure. From this simulation, the enthalpy of the vapor phase is obtained. A single-phase NPT simulation was performed at the vapor pressure with a starting density near the liquid phase density obtained from the two-phase NVT simulation. From this simulation, the enthalpy of the liquid phase is obtained. The enthalpy of vaporization was defined as the difference between the enthalpy of the vapor simulations and the enthalpy of the liquid simulations. The resulting data is shown in Figure 2.8. The data approaches zero as the system approaches the critical temperature, as expected. There is also good agreement with experimental values [24] for methane at all values of the reduced temperature with an average relative error of 2.2%.

2.4 Conclusions

In this chapter, a comparison is made between TQMD and VEMD for the VLE of a pure component Lennard-Jones fluid. A modified algorithm is used to generate a density distribution function, which is used to identify the liquid, vapor, and interfacial

regions. Earlier reports of comparable accuracy between the two methods are confirmed. The predictions of density, vapor pressure, enthalpy of vaporization, and critical properties from simulation were compared with an analytical equation of state[23] and experimental data[24,25] with good results. The transient behavior of the interface formation was examined during the equilibration of the simulation and the time constants associated with this process for both methods are reported as functions of temperature. VEMD equilibrates faster than TQMD to the bulk densities for this simple system.

Furthermore, it is shown that simulations using generic literature values for the potentials can generate VLE data that is in excellent agreement with experimental data when compared on a corresponding states basis, in which the temperature, pressure, and density are reduced by the experimental and simulated critical properties.

2.5 Acknowledgements

The authors gratefully acknowledge the financial support of the Office of Fossil Energy of the U.S. Department of Energy (DOE). This work was partially supported by the Office of Fossil Energy of the US Department of Energy (DOE) under contract # DE-AC05-00OR22725 to Oak Ridge National Laboratory (ORNL) through a subcontract at the University of Tennessee. ORNL is operated for DOE by UT-Battelle, LLC, under contract # DE-AC0500OR22725. This research used resources of the Center for Computational Sciences at ORNL through the University of Tennessee Computational Sciences Initiative.

Appendix A: Tables and Figures

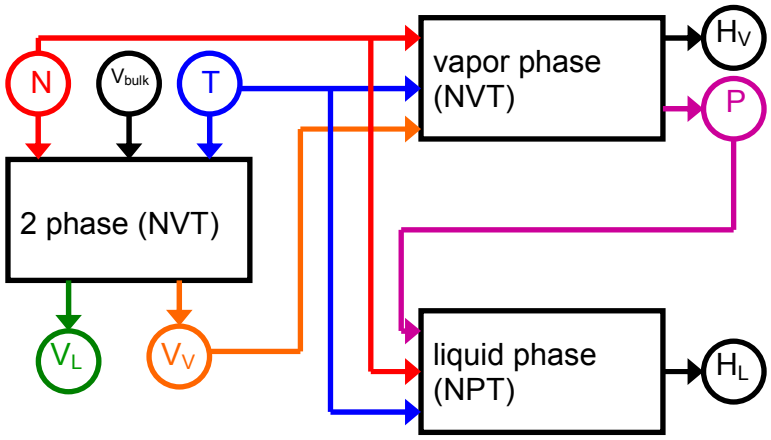

Figure 2.1: Simulation methodology used to find the coexisting vapor and liquid densities, the critical temperature, the critical density, the critical pressure, the vapor pressure, and the enthalpy of vaporization.

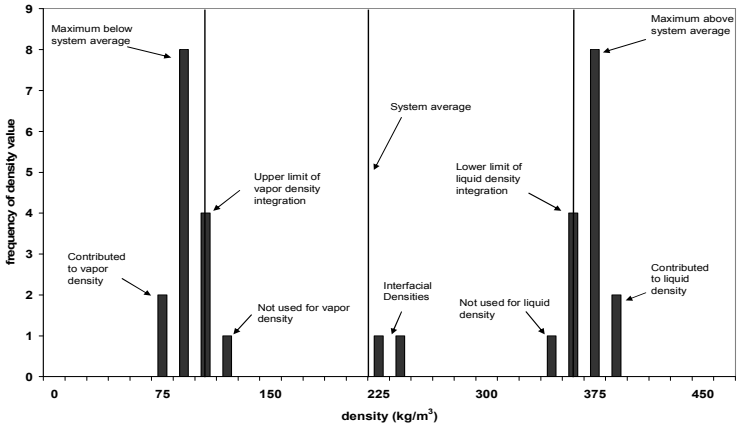

Figure 2.2: Explanation of method to determine vapor, liquid, and interfacial densities from a hypothetical histogram of the density distribution.

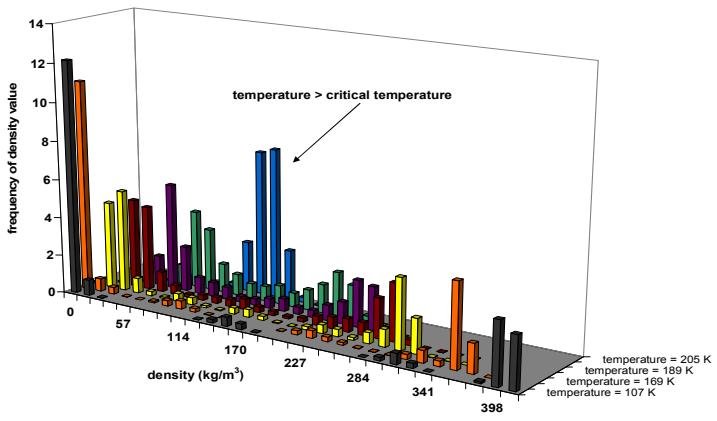

Figure 2.3: Inverted histograms for temperatures increasing to above the critical temperature. The temperature in the rear of the plot is a temperature greater than the critical temperature that gives a single-phase peak. The simulation method was VEMD for all of the histograms represented.

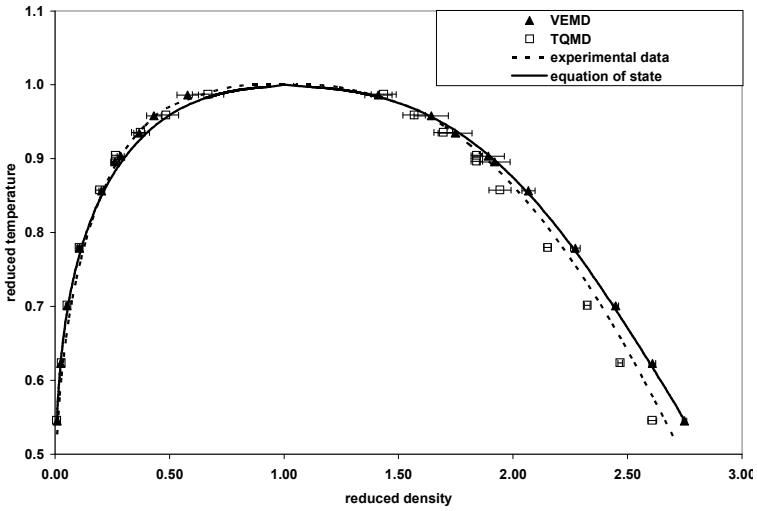

Figure 2.4: Resulting reduced vapor and liquid densities (ρ/ρ_c from both TQMD (squares) and VEMD (triangles) as functions of reduced temperature (T/T_c) the dashed line is experimental data[25] and the solid line is the equation of state[23].

Table 2.1: The resulting vapor density (ρ_v) and liquid density (ρ_L) and their errors are shown as functions of temperature (K) for the VEMD and TQMD methods.

	VEMD		TQMD	
T	ρ_L	ρ_V	ρ_L	ρ_V
K	kg/m^3	kg/m^3	kg/m^3	kg/m^3
195	211 ± 8	86 ±7	226 ± 8	105 ± 10
189	245 ± 11	64 ± 5	247 ± 8	76 ± 9
185	261 ± 11	54 ± 4	267 ± 7	59 ± 6
179	282 ± 10	42 ±2	290 ± 4	41 ± 3
177	287 ± 10	38 ± 3	290 ± 4	41 ± 3
169	309 ± 4	30 ± 2	306 ± 8	30 ±3
154	339 ± 3	15 ± 2	339 ± 2	16 ±1
139	365 ± 2	7 ± 1	367 ± 2	8.4 ± 0.6
123	389 ± 2	3.7 ± 0.3	389 ± 1	4.2 ± 0.5
108	410 ± 1	1.3 ± 0.4	411 ± 3	1.1 ± 0.2

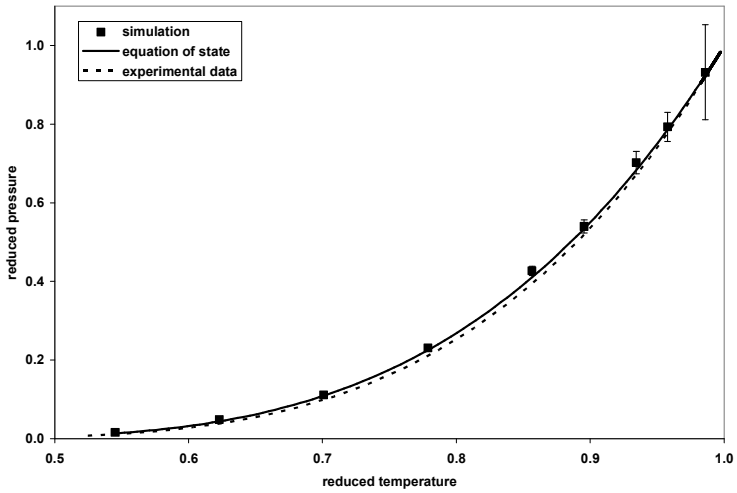

Figure 2.5: Reduced vapor pressure (P/P_c) as functions of reduced temperature (T/T_c) from single-phase simulations using the vapor densities of the VEMD model (squares). The dashed line is a fit of experimental data[25], and the solid line is the expected vapor pressures from the equation of state[23].

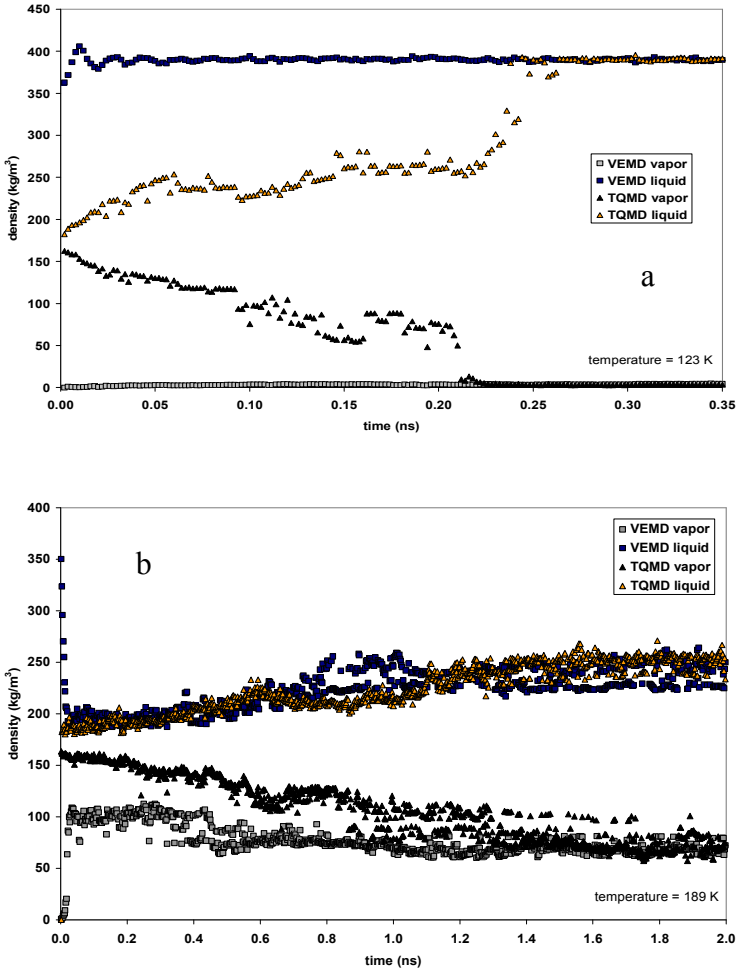

Figure 2.6: (a) Density data (kg/m^3) as functions of time (ns) during the equilibration step for a low temperature, T = 123 K. (b) Density data (kg/m^3) as functions of time (ns) during the equilibration step for a higher temperature, T = 189 K. The squares represent the data from VEMD, and the triangles represent data from TQMD.

Table 2.2: Relaxation times (ns) for each method for the vapor (τ_v) and liquid (τ_L) phases as functions of temperature (K).

	TQMD		VEMD	
T	τ_V	τ_L	τ_V	τ_L
K	ns	ns	ns	ns
108	5.1152E-02	2.1953E-02	6.1116E-04	3.8645E-04
123	4.4048E-02	2.2502E-02	1.7468E-03	3.3742E-04
138	4.8779E-02	4.1117E-02	1.5239E-02	8.7802E-03
154	1.4386E-01	3.1031E-01	2.3019E-02	3.9592E-03
169	2.8299E-01	3.0011E-01	3.1135E-02	7.3638E-02
177	2.1560E-01	3.3605E-01	2.2245E-02	1.2432E-01
185	3.2441E-01	6.2162E-01	1.5758E-02	7.8752E-02
189	8.0933E-01	8.2059E-01	1.3966E-01	1.2334E-01
195	1.0486E+00	1.3428E+00	1.2351E-01	3.0308E-01

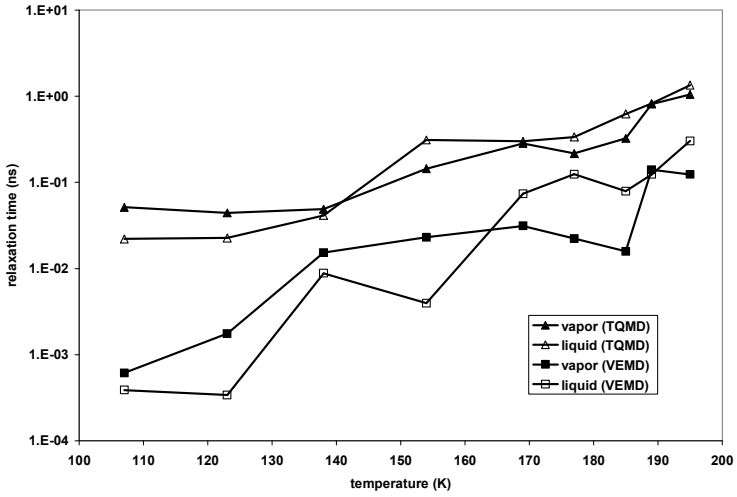

Figure 2.7: The resulting relaxation times (ns) for the transient density data as functions of temperature (K).

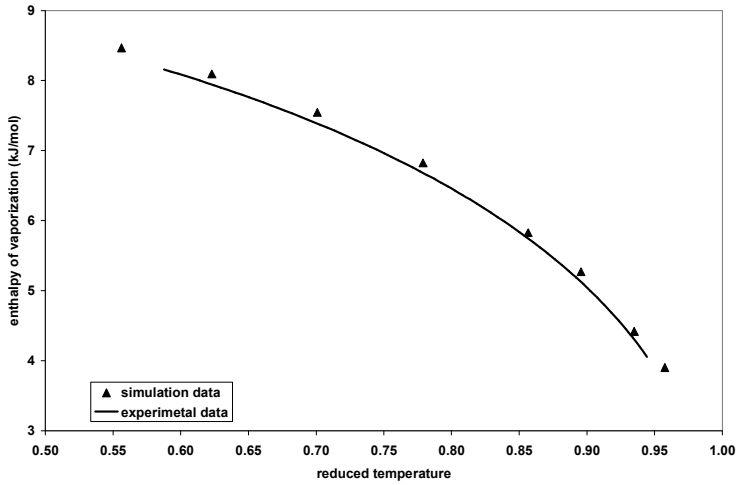

Figure 2.8: Enthalpy of vaporization (kJ/mol) for the VEMD model as functions of reduced temperature (T/T_c). The solid line is a fit of experimental data[24].

CHAPTER 3

Measuring Coexisting Densities from a Two-phase Molecular Dynamics Simulation by Voronoi Tessellations

This chapter is a slightly revised version of a paper by the same title published in the Journal of Physical Chemistry, Section B: 2007 by Jared Fern, David Keffer, and William Steele:

J. Fern, D. Keffer, and W. Steele, *Measuring Coexisting Densities from a Two-phase Molecular Dynamics Simulation by Voronoi Tessellations,* J. Phys. Chem. B. **111** (13), 3469 -3475, 2007

The use of "we" in this chapter refers to the co-authors and the author of this dissertation. My primary contributions to this paper include: (1) development of the algorithm, (2) creating programs to perform the Voronoi Tessellation, (3) all of the simulation work, and (4) all of the figure generation, and writing.

Abstract

A new algorithm is presented that allows for the determination of bulk liquid and vapor densities from a two-phase Molecular Dynamics (2ϕMD) simulation. This new method does not use any arbitrary cut-offs for phase definitions; rather it uses single-phase simulations as a self-consistency check. The method does not use any spatial bins for generating histograms of local properties, thereby avoiding the statistical issues associated with bins. Finally, it allows one to approach very close to the critical point. The new method utilizes Voronoi tessellations to determine the molecular volume of every point at every instance in a molecular dynamics simulation. Since the molecular volume is calculated throughout the simulation, statistical parameters such as the average molecular volume and average molecular variance are easy to obtain. In order to define the phases, the normalized variance of the molecular volume from 1ϕMD and 2ϕMD is used as a self-consistency check. The new method gives new insight into the nature of the near-sub-critical fluid. The critical properties from this analysis are $T_c = 1.293$ and $\rho_c = 0.313$. Direct simulation of the two-phase system was performed up to a temperature of 1.292. The results show excellent agreement to experimental results and Gibbs Ensemble Monte Carlo for coexisting densities. We see that well below the critical temperature, some particles are neither liquid nor vapor. These interfacial particles are primarily, but not exclusively, concentrated at the bulk interface. However, as we approach the critical point, some particles are considered both liquid and vapor. These interfacial particles are distributed through the system

3.1 Introduction

There are a variety of tools available for the study of Vapor-Liquid Equilibrium (VLE). Aside from experimental measurements, computational methods have been evolving since the mid 1970s. Ladd and Woodcock[8] and Chapela *et al.* [7] studied VLE by simulating a slab of liquid and a slab of vapor to find the surface tension and the equilibrium densities by Molecular Dynamics (MD). The work of Ladd and Woodcock was then extended upon by Holcomb *et al.*[36].

Along with these examples for MD simulations, there are many additional ways to simulate VLE. One common method to study phase equilibrium is by Gibbs Ensemble Monte Carlo (GEMC) [6,9]. GEMC simulates the bulk liquid and bulk vapor in separate boxes and the molecules are allowed to exchange between the boxes. The simulation strives to maintain a constant chemical potential, temperature, and pressure between the two boxes. One other method of direct simulation of vapor liquid equilibrium is the NPT + test particle method created by Lofti and coworkers[37]. This method is implemented by conducting an MD simulation in the isothermal-isobaric ensemble (NPT) coupled with the Widom particle insertion method[38] to obtain the chemical potential of the system. Simulations are performed for both the liquid and vapor phases independently, and the results are then used to calculate the points on the two-phase envelope.

There are also indirect methods to obtain phase equilibrium. These indirect methods use an established state point and then use statistical methods to obtain the rest

of the two-phase region close to the critical point. These methods include histogram reweighting techniques [39,40] and Gibbs-Duhem integration [6].

The two primary methods available to simulate directly the phase diagram are two-phase Molecular Dynamics (2ϕMD) and GEMC. There are known deficiencies with the GEMC methods as mentioned by Gelb and Müller[10]. Equilibration is difficult to achieve when simulating dense phases because of the poor statistics associated with the insertion/deletion steps. The GEMC methods are difficult to apply to systems containing very complex molecules without substantial modifications, and are also difficult to implement on parallel computers. In addition to these deficiencies, GEMC simulations can have problems as the simulation approaches the critical temperature because the identity of the volumes can swap during the simulation [6]. When this occurs the results are then analyzed by the distribution of a given density in the simulation.

Simulating VLE with MD in the canonical (NVT) ensemble can potentially overcome all of the limitations of GEMC. In addition, complex fluids are routinely handled and MD codes are particularly amenable to parallelization. Perhaps more importantly, by simulating the interface, MD simulations allow for the investigation of interfacial properties such as molecular orientation, diffusion of molecules through the interface, and thickness of the interface. Furthermore, one can observe the dynamics of interface formation and destruction in MD simulations.

In the last few years, there have been two different methods developed to study VLE with MD. These two methods are Temperature Quench Molecular Dynamics (TQMD) and Volume Expansion Molecular Dynamics (VEMD). TQMD, as

implemented by Gelb and Müller [10], allowed for the simulation of the liquid and vapor phases in the same simulation cell. The system is equilibrated at a temperature above the critical temperature and density; then suddenly cooled into a region of mechanical and thermodynamic instability. The system then separates into liquid and vapor phases separated by an interface. VEMD, used by Pamies *et al.*[12], also allowed the simulation of the vapor and liquid phases to be simulated in the same cell. This method is analogous to a piston experiment where a volume of liquid is suddenly expanded to separate into liquid and vapor phases. The VEMD model starts as an equilibrated liquid then the simulation cell is suddenly expanded to give a density in the unstable region along the line of rectilinear diameter. The system then divides into vapor and liquid phases separated by an interface.

The above methods are two different ways to obtain a two-phase system by molecular dynamics. The more difficult task associated with 2ϕMD (and absent in low temperature GEMC) is extracting the values for the bulk liquid and vapor densities. Gelb and Müller[10] and Martínez-Veracoechea and Müller [11] cut the simulation volume into boxes and determined average coordination numbers of each box; then placed the average coordination numbers into an inverse histogram. The maximum repeated values are then used with a phase cut-off to determine the density of each phase. Example phase cut-offs are: (1) the liquid phase has a coordination number greater than 4, and (2) the vapor phase has a coordination number less than 2. The resulting procedure has four adjustable parameters for the determination of the phases. These four parameters are the distance cut-off for coordination number, spatial bin size, density bin size for the probability

distribution function, and phase cut-offs of the maximum values in the distribution function.

The use of bins presents statistical problems when creating a probability distribution of a local property. One would like to have as many bins as possible to obtain the best statistical representation, but in the limit of very small bins, the resulting density distribution is either 1 or 0 because the bin is either occupied or unoccupied, which presents no useful information regarding the densities of the phases. The other extreme is that in the use of very large bins, the resulting density profile is that of the total system, which provides no useful information on the phase equilibrium. The hope is that there exists an intermediate sized bin from which the best VLE data possible can be extracted. The optimal bin size, if it exists at all, is probably functions of thermodynamic state. This problem associated with bins makes the extraction of reliable VLE data from 2ϕMD fraught with effects due to arbitrarily chosen bin-size. These problems are eluded to by Martínez-Veracoechea and Müller [11]. In the literature, these issues have been partially overcome by the use of very large (500,000 particle) simulations [10,11]. It is also important to note that the use of very large systems can also be used combat to finite size effects as the system approaches the critical point.

One other method to determine the bulk vapor and liquid densities is to fit the density profile along the axis normal to the interface to a hyperbolic tangent function[7]. The function contains four adjustable parameters. The use of the hyperbolic tangent function relies upon a planar interface being present, along with no local effects due to obtaining the two-phase system, such as explosive boiling, and the center of mass of the

liquid droplet remaining stationary. Since the function only allows for planar interfaces, the investigation of densities close to the critical temperature is not an option since there is no guarantee that the interface will be planar. Also, the fitting of the function loses all information about any other local phenomena.

In order to correct the above deficiencies, a method is presented that utilizes Voronoi tessellations (VT) to determine the volume of every particle in the simulation cell. This method is free of all arbitrary choices by the user and can be easily implemented in any system. Furthermore, the method will link the two-phase simulations back to single-phase simulations by the normalized variance of the molecular volume as determined from the Voronoi tessellation. This link will be used as a self-consistency check to insure that the correct values for the density are obtained, thus removing all arbitrary choices in phase definition. The new method is also capable of giving new insight to the phenomena that occurs as the temperature approaches the critical point.

3.2 Voronoi Tessellation

Voronoi tessellations (VT) have wide applications and have been utilized to obtain information pertaining to stellar bodies [14], free volumes in proteins[15], crystal deformations[5], the properties of neurons[41], in the physics of hard-sphere fluids[42,43] in addition to many other applications[16]. For a thorough reference of the history of VT, see the review by Aurenhammer[14].

VT is a procedure that takes as input a set of points in a volume (either periodic or bounded) and divides the volume into sub-volumes or cells associated with each point, such that all of the volume associated with a point is geometrically closer to that point than to any other. The sub-volumes are only functions of the distance to the nearest neighbors of every point. An illustration of this procedure is shown in Figure 3.1.

Figure 3.1 shows the resulting sub-volumes for a simple periodic system in two dimensions. The dotted lines represent the nearest neighbors around every point, the x's are the vertices from the VT defining the sub-volume, and the solid lines connect the vertices around each point.

When applied to a system at the molecular level, VT leads to a molecular volume for every particle. From this set of molecular volumes, V_n^i, we can obtain, among other statistical properties, the mean molecular volume, $\overline{V_n}$, and the variance of the molecular volume, $\sigma_{V_n}^2$. Each particle is in a Voronoi cell, which in effect is its own custom-sized bin. However, the size of the bin is different for each particle because it is uniquely defined by the VT.

3.3 Phase Determination

In order to locate "bulk liquid" and "bulk vapor" phases within the 2ϕMD simulation, an iterative procedure is used. First, one guesses (i) the upper limit of the average liquid molecular volume so that all molecules with volume less than that limit are

defined as liquid and (ii) the lower limit of the vapor molecular volume so that all molecules with volume greater than that limit are defined as vapor. Based on these limits, one calculates the liquid statistical measures, $\overline{V_n^L}$ and $\sigma^2_{V_n^L}$, based on only those particles defined as liquid. The same procedure applies for the vapor statistical measures, $\overline{V_n^V}$ and $\sigma^2_{V_n^V}$.

At this point a self-consistency check must be used to determine the validity of our arbitrarily chosen limits on the molecular density of each phase. This check is simple: two one-phase Molecular Dynamics (1ϕMD) simulations are performed at the same temperature as the 2ϕMD simulation and at the molar volume given by $\overline{V_n^L}$ and $\overline{V_n^V}$. From the 1ϕMD simulations $\sigma^2_{V_n^L}$ and $\sigma^2_{V_n^V}$ is computed. If the value of $\sigma^2_{V_n^L}$ and $\sigma^2_{V_n^V}$ from 1ϕMD match those from 2ϕMD within an acceptable tolerance, then the choice of phase limits was appropriate. Otherwise, one must choose new phase limits and iterate. It is important to point out that each step in the iteration requires a new 1ϕMD simulation (which can be a relatively small system) but not another 2ϕMD simulation (which typically must be much larger), as long as the Voronoi volumes from a set of configurations were saved during the 2ϕMD simulation.

Figure 3.3 shows an example of this iterative procedure for the liquid and vapor phases, in which the normalized variance of the molecular volume is denoted as $\kappa_1^L \equiv \sigma^2_{V_n^L} \Big/ \overline{V_n^L}$ and $\kappa_1^V \equiv \sigma^2_{V_n^V} \Big/ \overline{V_n^V}$. The subscript 1 indicates that this is an averaged single particle property. The 2ϕMD curve was generated from a single simulation,

changing only the phase limit until the two lines intersected. The 1ϕMD curve was generated from multiple simulations at varying molar volumes. It can be seen that this combination of 1ϕMD and 2ϕMD provides an unambiguous determination of the phase limits and the corresponding phase properties.

3.4 Results and Discussion

As an example system, a simple Lennard-Jones (LJ) fluid is considered, which has been very well studied. The important simulation parameters are as follows: 8000 particles were simulated; a cut-off was employed beyond 6 LJ diameters for the interaction potential [12,44,45], and data was collected for 2 ns after equilibration. The results are presented in reduced Lennard-Jones units [5].

We include no long-range correction to energy or pressure, because we have a large cut-off distance. There are methods available in the literature to compensate for the long-range corrections in an inhomogeneous system[33], but these methods require there to be a planar interface. The simulations were performed by using TQMD, so it is uncertain if a planar interface would be present. It is also shown from our results that the 2ϕ system has a diffuse and non-contiguous interface, which grows more diffuse as the system approaches the critical temperature.

The simulations were performed using a rigorously tested, in-house designed, parallel MD code. The simulations used a Nosè-Hoover thermostat[26,46] and a fifth-order Gear Predictor-Corrector[28,29]. The Voronoi analysis was also performed on an in-house

designed parallel code using the properties of Voronoi diagrams mentioned by O'Rourke[16].

In order to implement the Voronoi Tessellations in an MD simulation, a periodic simulation cell is used with the minimum image convention, the triangulation is performed on the center of mass of Lennard-Jones spheres, and the analysis is performed after the simulation was completed on saved configurations. The speed of the analysis was increased by truncating a sorted neighbor list. The total volume of the simulation cell was used as a check to determine if enough neighbors were used in the analysis. The summation of the individual molecule volumes equals the total simulation volume to machine precision.

In order to ensure that the simulations were equilibrated, the simulations at low and intermediate temperatures (T* = 0.90 to 1.20) ran for 5.15 ns before data production. The simulations at higher temperatures (T* = 1.20 to 1.27) equilibrated for 8.2 ns and at the highest temperature (T* = 1.29) equilibration lasted for 11.20 ns. The potential energy was monitored throughout the simulation to gauge whether the positions of the molecules in the system had equilibrated, and the equilibration of particle volumes was determined by monitoring the variance of the Voronoi volume over all particles. In addition, the vapor and liquid densities were calculated via the procedure described here every 0.1 ns, which showed that the densities fluctuated about constant values with time.

In Figure 3.4, the probability distributions of the molecular density from the converged 1ϕMD and 2ϕMD simulations at various temperatures are shown. All temperatures are below the critical point. Good qualitative agreement is seen between the

1ϕMD and 2ϕMD distributions for the liquid and vapor. It is important to note that the 1ϕMD and 2ϕMD distributions for each phase have the same mean molecular volume and the same variance of the molecular volume. Clearly, the shapes of the distributions do not match exactly.

Well below the critical temperature, as shown in Figure 3.4(a), there is a set of molecules that are neither vapor nor liquid, which we can consider as interfacial molecules. Interestingly, as one approaches the critical point, the distributions of the vapor and liquid phases from the independent single-phase simulations overlap. Consequently, in the 2ϕMD simulation at temperatures below but near the critical temperature, the lower density limit of the liquid is less than the upper limit of the vapor. As a result, some particles are considered as both vapor and liquid. In other words, in a near critical fluid, there are liquid regions, vapor regions, and regions that can be considered as both liquid and vapor.

In Figure 3.5, a series of snapshots are shown of equilibrated 2ϕMD simulations at multiple temperatures, all below the critical point. We color the atoms by phase: particles in the liquid phase are green and particles in the vapor are red. At low temperatures (T less than 1.20), particles that are neither vapor nor liquid are blue. At high temperatures (T greater than 1.20), particles that are both vapor and liquid are blue. It can be seen that the use of VT allows for define vapor and liquid phases to be defined *that are not contiguous*. This is an important advantage of using VT to define local density rather than the conventional use of spatial bins, because as one nears the critical point, one does not expect to find contiguous phases. This presents the possibility that

the use of VT will allow this simulation technique to continue to provide good VLE data closer to the critical point than other methods.

In Figure 3.5(a - c), it is shown that far below the critical temperature, there are bulk liquid and vapor regions. The interfacial atoms are located primarily at the bulk interface but also are scattered through the bulk phases. This scattering of interfacial particles (by defining the interface as neither bulk vapor nor bulk liquid) is a result of the VT procedure. Were one to use spatial bins and define all molecules in the predominantly green region as liquid or the predominately red region as vapor, one would obtain higher vapor densities and lower liquid densities. This procedure suggests that "interfacial" particles are concentrated at, but not limited to, the bulk interface. As the temperature is increased in Figure 3.5(d - f), it is shown that there are no longer any interfacial atoms. All atoms are either bulk liquid, bulk vapor, or both bulk liquid and bulk vapor. It can be seen that those atoms with molecular volumes corresponding to both bulk liquid and bulk vapor are not concentrated at the interface of the predominately liquid and predominately vapor regions, but rather are scattered throughout the system.

In Figure 3.6, we show the vapor-liquid phase diagram for this system. In the plot, we compare (i) the result of our method, (ii) the results from GEMC simulation[11], (iii) results from a 32-parameter EOS fit to extensive simulation data[23]. We see that our new method provides excellent agreement with GEMC. We also see that our algorithm containing 2ϕMD and 1ϕMD simulations allows one to obtain properties much closer to the critical point. GEMC has difficulty simulating close to the critical temperature because the identity of the liquid and vapor phases can swap during the

simulation[6]. Near the critical point, there is non-negligible disagreement between the simulation results (2ϕMD or GEMC) and the LJ-EOS. Since the two independent simulation methods agree, we believe that this disagreement between simulation and EOS is likely due to limitations in the LJ-EOS based on the quality of simulation data to which it was fit.

Finally, Figure 3.7 presents a comparison between our results from the algorithm containing 2ϕMD and 1ϕMD simulations with experimental results for methane [25], which is reasonably well approximated as a Lennard-Jones fluid. While one might expect simulation results of a LJ fluid to match an EOS fit to simulation data better than experiment, here we observe the contrary behavior.

The critical temperature of this system is 1.293 and the critical density is 0.313 in reduced units as determined by the law of rectilinear diameter and by the Ising scaling with the classical critical exponent of 0.32[6]. The critical temperature of the Lennard-Jones EOS is 1.316 and the critical density is 0.304. The resulting percentage errors are 1.7% for the critical temperature and 3.0% for the critical density. The LJ EOS may overestimate the critical point and coexisting densities at high temperatures. There were only two sets of data used to perform the fit in the critical regime [23]. One of the sets of data was the NPT + test particle method of Lofti[37]. It is possible that the Lofti data over predicted the breadth of the phase envelope because it is very difficult to simulate in the NPT ensemble along the two-phase region and simulated just outside the two-phase region. This is because the system can drift to vapor from liquid and liquid to vapor. If one uses the LJ EOS to calibrate the arbitrary phase definition, one can find better

agreement with the LJ EOS, resulting in a systematic deviation from our simulation results, which are free of arbitrary choices.

If methane is considered as the fluid with σ = 3.73 Å and ε = 148 K[12], the resulting critical temperature is 191.4 K and the critical density is 161.0 kg*m^{-3}. The accepted experimental values for the critical temperature of methane is 190.5 K and the critical density is 162.6 kg*m^{-3}. Our percent error relative to the experimental critical temperature is 0.4% and our percent error relative to the critical density is 1.1%. It is felt that the good agreement seen as compared to the experimental data validates our conclusions concerning the LJ EOS.

We should point out that we can use a smaller number of particles (8000) with VT as compared to 500,000 particles used to counter the statistical problems associated with spatial bins [10,11]. Another reported advantage of the large system size is that it combats the system size effects that can occur as the temperature approaches the critical point. Our new method does not appear to be as affected by finite size effects, because phase definition is based on highly localized properties (single-particle molecular volume and single-particle molecular volume variance).

This technique is directly extendable to phase equilibrium of mixtures, in which limits for the density of each species in each phase must be iteratively determined. It is also directly applicable to polyatomic fluids, since the VT can be applied to individual atoms and then summed over all atoms in a molecule to yield the molecular volume.

3.4.1 Equivalency of κ_1 across Simulations and Ensembles

Since κ_1 is being used as a criterion for defining the phases, it is important to establish that the measured value of κ_1 is independent of the size of the system and the ensemble in which the simulation is performed. In Figure 3.8 the normalized variance per particle as functions of cluster size for 3 single-phase simulations in the NpT ensemble with N = 1000, 4096 and 8000 particles and for 1 single-phase simulation in the NVT ensemble with N = 8000 particles is plotted. Clusters were formed by randomly grouping molecules (without any regard for position). Thus a simulation with N= 8000 had 8000 clusters of size 1 and it had 2 clusters of size 4000.

The crucial point in Figure 3.8 is that for all simulations, regardless of size or ensemble, the value of the normalized variance per particle is the same for a cluster size of one. Therefore the single-particle property, κ_1, is independent of system size and ensemble. This is important because the phase criteria is based upon a comparison of κ_1 from a 1ϕMD simulation in the NVT ensemble of N = 1000 with κ_1 from a 2ϕMD simulation, where the volume and number of particles in each phase vary from one configuration to the next.

At cluster sizes larger than one, the normalized variance per particle is functions of system size and ensemble. If we take this to the limit where we have 1 cluster composed of all of the particles in the simulation, then we find that variance in the NVT simulation goes to zero, as it must since the total volume is constant. The variance in the NpT ensemble goes to a value independent of system size, once a minimum system size

is used. This is consistent with fluctuation theory, which states that the isothermal compressibility, given by [5]

$$\beta_T = \frac{1}{k_B T} \frac{\left\langle \delta Vol^2 \right\rangle_{NPT}}{\left\langle Vol \right\rangle} \tag{1}$$

is a function of the normalized variance of the volume per particle.

Part of our motivation in choosing the mean and the variance of the Voronoi volume as criteria for the phase definitions in 2ϕMD simulations was the fact that these two properties are local properties. The normalized variance of the single-particle molecular volume, κ_1 and the isothermal compressibility from fluctuation theory, share the same functional form, but they are not representative of the same property (since the former assumes a cluster size of 1 and the latter a cluster size of N). It is nevertheless interesting to note that the bulk isothermal compressibility is itself a highly localized function, as evidenced by the fact that, in the Ornstein-Zernike closure, the isothermal compressibility is strictly functions of the short-ranged direct correlation function[47].

3.5 Conclusions

A new method is presented to account for the statistical problems associated with the use of bins in 2ϕMD simulations. The new method utilizes Voronoi tessellations to obtain the molecular volumes for every particle simulated. The resulting mean and variance of the molecular volumes are then used to self-consistently determine the phases. There is excellent agreement between this work and GEMC simulations far from

the critical point, where GEMC data is available. We have excellent agreement with experimental results up to and including the critical point. The new algorithm also allows for new insight as the system approaches the critical temperature since at every instant in time one can know if a molecule is in the liquid or vapor phase regardless of the location of the interface. We see that well below the critical temperature, some particles are neither liquid nor vapor. These interfacial particles are primarily but not exclusively concentrated at the bulk interface. However, as we approach the critical point, some particles are necessarily both liquid and vapor. These interfacial particles are distributed through the system.

3.6 Acknowledgements

The authors gratefully acknowledge the financial support of the Office of Fossil Energy of the U.S. Department of Energy (DOE). Through the UT Computational Science Initiative, this research project used resources of the Center for Computational Sciences at Oak Ridge National Laboratory, which is supported by the Office of Science of the DOE under Contract DE-AC05-00OR22725.

Appendix A: Figures

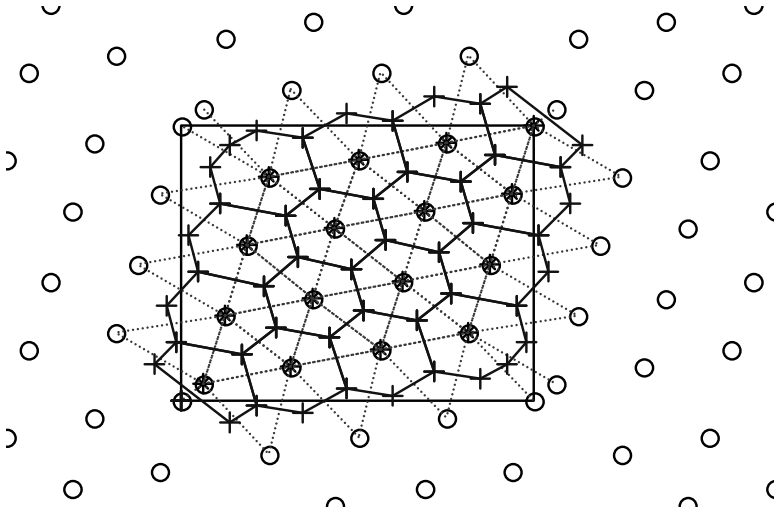

Figure 3.1: An illustration of a Voronoi tessellation in a two dimensional, periodic simulation cell. The circles represent the molecules, the dashed lines are the nearest neighbors of each molecule, the x's are the vertices which define the sub-volume of each molecule, and the solid lines connect the vertices.

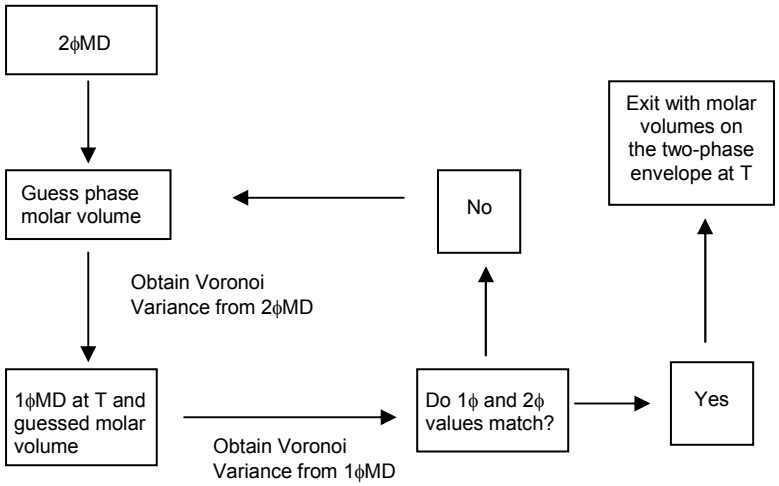

Figure 3.2: Flow sheet describing the procedure to determine the molar volumes of the vapor and liquid phases at each temperature.

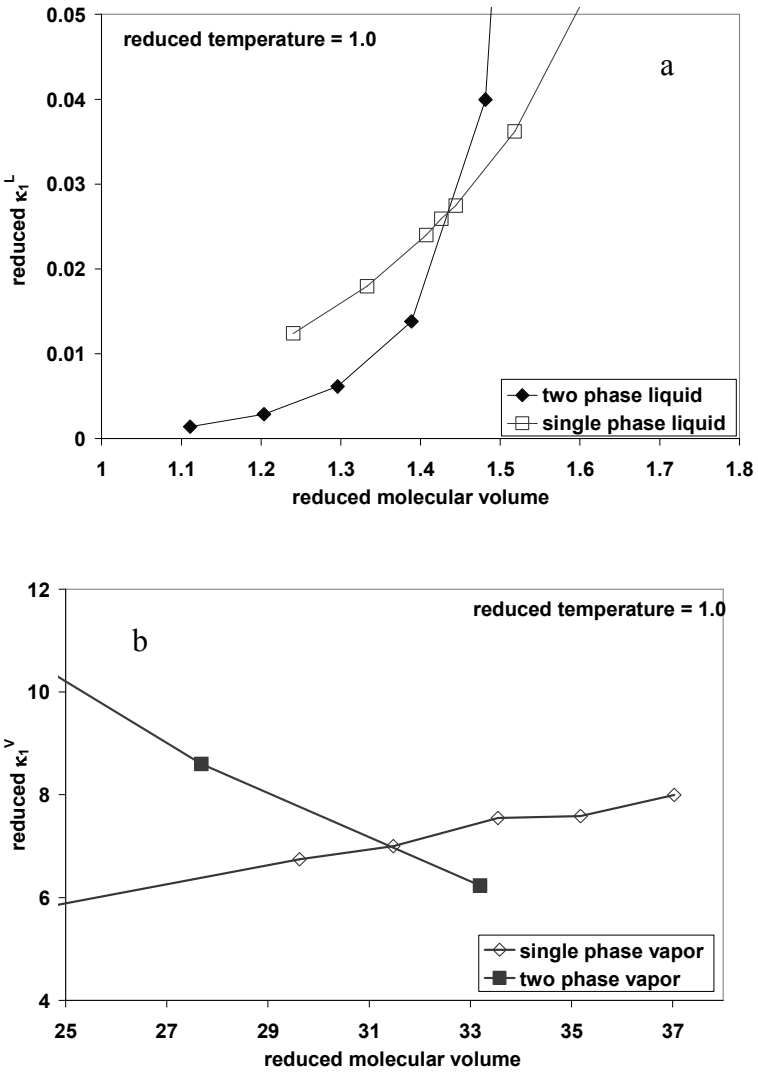

Figure 3.3: The intersection of the 2ϕ molar volumes and the 1ϕ molar volumes as functions of the normalized variance of the average molar volume denoted by κ_1 for (a) liquid and (b) vapor.

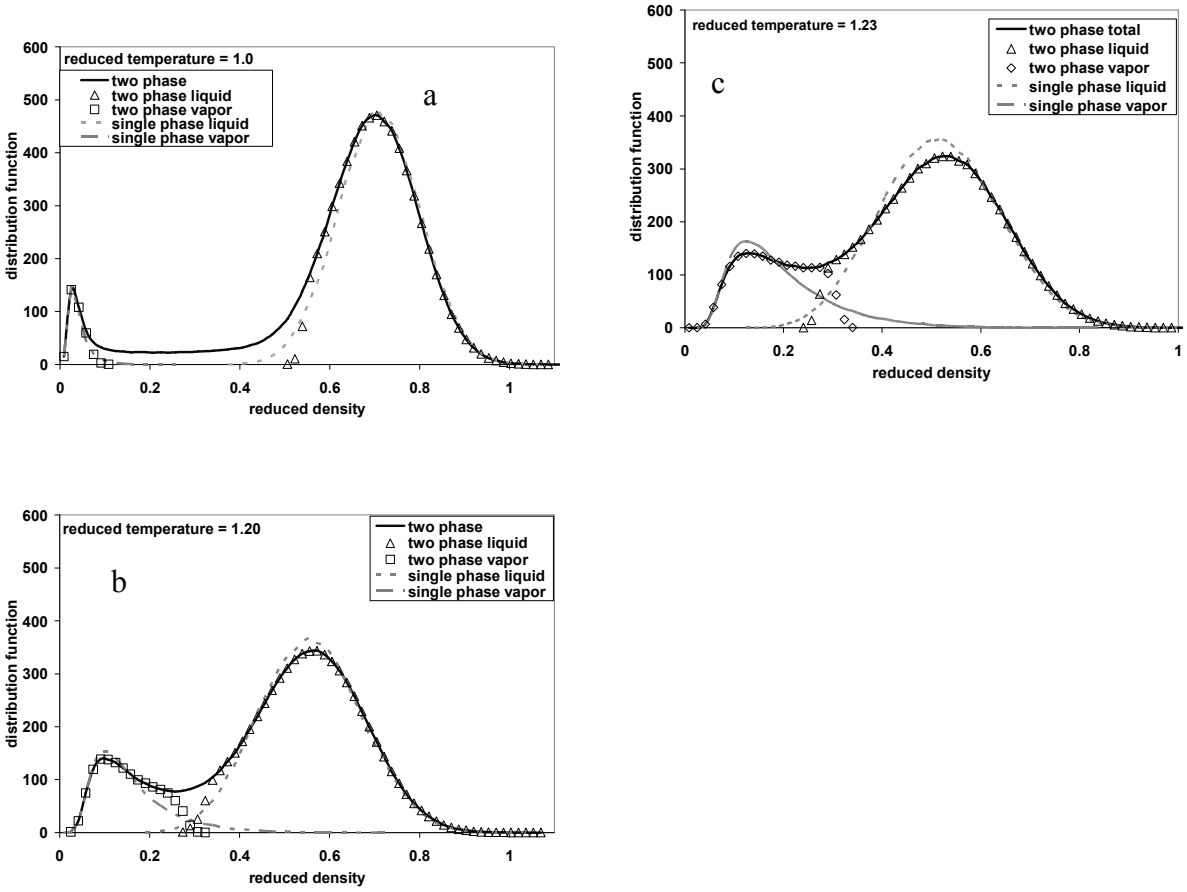

Figure 3.4: The unnormalized distribution of molecules in the 2ϕ simulation (solid line); the results from the procedure for the liquid (triangles) and vapor (boxes) phases, and the 1ϕ liquid and vapor simulations (dashed lines). Reduced temperature is (a) 1.0, (b) 1.2, and (c) 1.23.

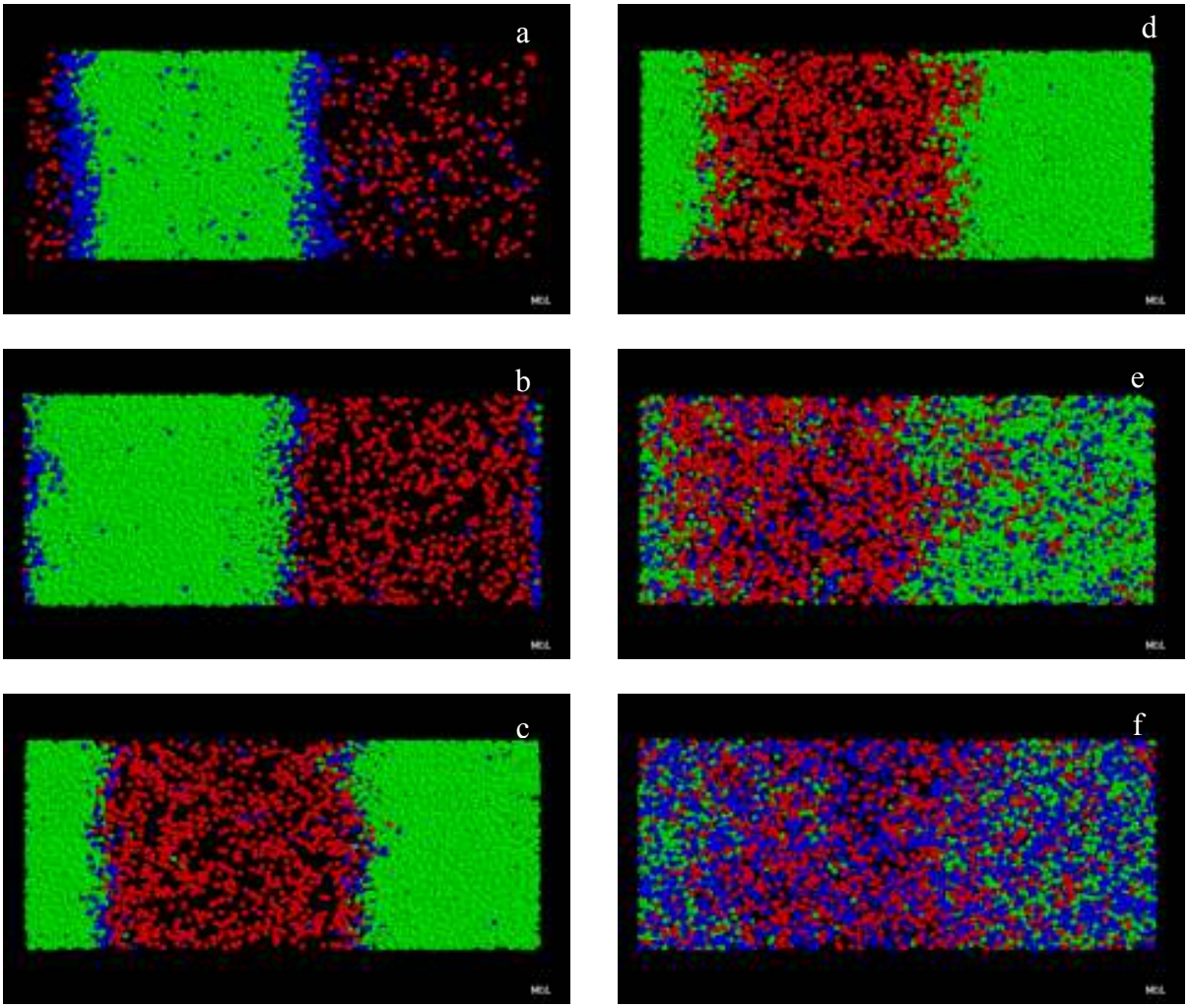

Figure 3.5: A snapshot of the final configuration for a reduced temperature of (a) 1.0, (b) 1.10, (c) 1.15, (d) 1.20, (e) 1.27, and (f) 1.29. In all plots, green represents the liquid molecules and red represents the vapor molecules. At the temperatures at and below 1.20 blue molecules are interfacial (neither liquid nor vapor) and at the high temperatures (above 1.20) blue molecules are both vapor and liquid.

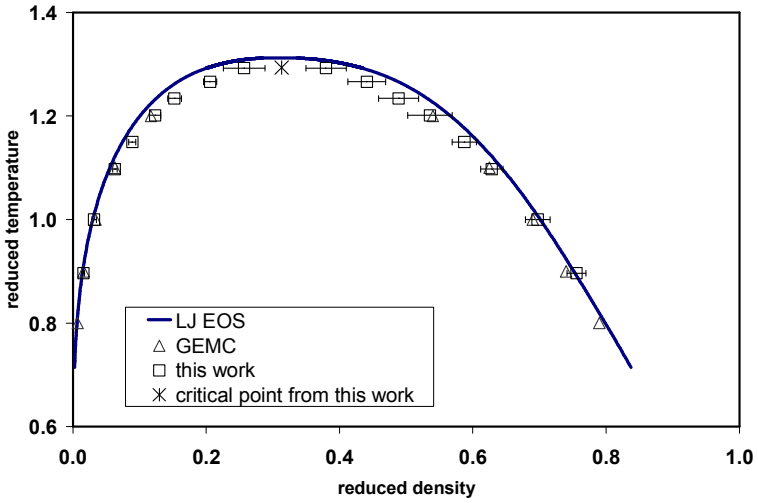

Figure 3.6: The phase diagram. The solid line is the Lennard-Jones Equation of State (EOS) [23]; the triangles are results from Gibbs Ensemble Monte Carlo [11]; and the boxes are the results from this work The critical point as determined from the fit from this work is designated with an asterisk.

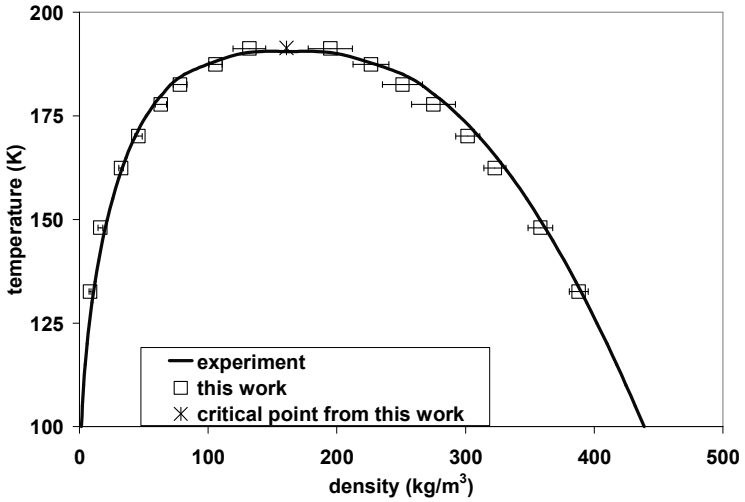

Figure 3.7: The phase diagram. The solid line is the experimental data for methane [25], and the boxes are the results from this work.

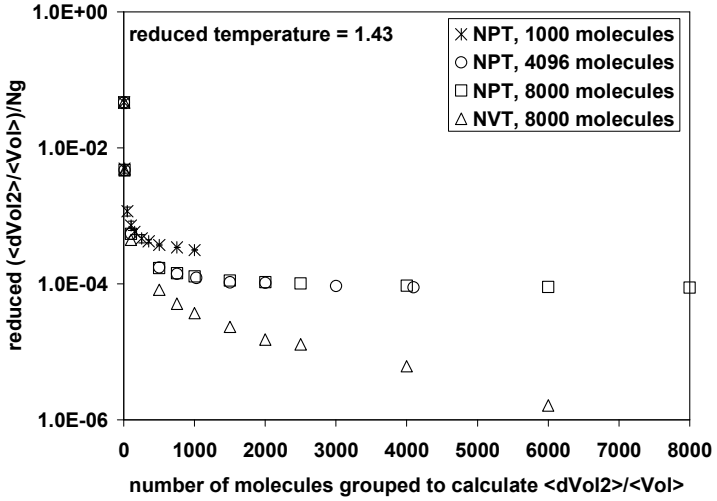

Figure 3.8: The normalized variance per particle as functions of cluster size for 3 single-phase simulations in the NpT ensemble with N = 1000 (asterisks), 4096 (circles) and 8000 (boxes) particles and for 1 single-phase simulation in the NVT ensemble with N = 8000 (triangles). Ng is the group size.

CHAPTER 4

Vapor-Liquid Equilibrium of Ethanol by Molecular Dynamics Simulation and Voronoi Tessellation

This chapter is a slightly revised version of a paper by the same title published in the Journal of Physical Chemistry, Section B: 2007 by Jared Fern, David Keffer, and William Steele:

J. Fern, D. Keffer, and W. Steele, *Vapor-Liquid Equilibrium of Ethanol by Molecular Dynamics Simulation and Voronoi Tessellation,* J. Phys. Chem. B. accepted for publication.

The use of "we" in this chapter refers to the co-authors and the author of this dissertation. My primary contributions to this paper include: (1) created code to simulate the OPLS-AA potential, Electrostatic Interactions, Radial Distribution functions, (2) all of the simulation work, and (3) all of the figure generation and writing

Abstract
Explicit atom simulations of ethanol were performed by molecular dynamics using the OPLS-AA potential and reaction field for the electrostatic interactions. The phase densities were determined self-consistently by comparing the distribution of Voronoi volumes from two-phase and single-phase simulations. This is the first demonstration of the use of Voronoi tessellation in two-phase molecular dynamics simulation of polyatomic fluids. This technique removes all arbitrary determination of the phase diagram by using single-phase simulations to self-consistently validate the probability distribution of Voronoi volumes of the liquid and vapor phases extracted from the two-phase molecular dynamics simulations. Properties from the two phase simulations include: critical temperature, critical density, critical pressure, phase diagram, surface tension, and molecule orientation at the interface. The simulations were performed from 375 Kelvin to 472 Kelvin. Also investigated were the vapor pressure and hydrogen bonding along the two phase envelope. The phase envelope agrees extremely well with literature values from GEMC at lower temperatures. The combined use of two-phase molecular dynamics simulation and Voronoi tessellation allows us to extend the phase diagram toward the critical point.

4.1 Introduction

The molecular simulation of Vapor-Liquid Equilibrium (VLE) is a powerful tool used to determine physical properties where experimental measurements cannot. The

most common method to simulate VLE is by Gibbs Ensemble Monte Carlo (GEMC)[6,9,20]. GEMC is a simulation method that allows one to simulate a vapor and a liquid in separate simulation volumes simultaneously to obtain phase equilibrium by matching chemical potentials in the vapor and liquid phases. There are many additional techniques available to measure VLE by molecular simulation. These methods include: Histogram reweighting[6,9], Gibbs-Duhem Integration[6,48,49], NPT + test particle[37], the Grand Equilibrium method[50], and Molecular Dynamics (MD)[7,8,10-13,33,50].

The use of MD to simulate VLE is different from all of these methods because in an MD simulation the vapor and the liquid are in the same simulation box separated by an interface. The presence of the interface greatly complicates the measurement of the vapor and liquid densities from a two-phase system, but it allows for the investigation of important interfacial properties, such as the surface tension, at the molecular level.

One of the challenges associated with two-phase MD simulation is the determination of distinct liquid and vapor phases and their respective properties, such as density. A variety of approaches have been used to determine densities from a two-phase MD simulation. These techniques include fitting a hyperbolic tangent function to determine the average vapor and liquid density[5,7,33,36,51]. Fitting the average density profile requires no center of mass movement and a planar interface, so it is not applicable to all systems of interest. The problems with this method arise when the temperature of the system is approaching the critical temperature, at which point the planarity of the interface is lost. The fitting also removes any extraction of data from the individual phases.

An additional method to determine the vapor and liquid densities is that of Gelb and Müller[10] and Martinez-Veracoechea and Müller[11]. This method involves determining a local parameter that describes the phase (such as the coordination number) and cutting the simulation volume into small spatial boxes. The average of the parameter within each box is then placed into an inverse histogram giving a distribution of the parameter within the simulation volume. Phase cut-offs are then used to determine the average vapor and liquid densities from the distribution function. The method still works if there is center of mass movement and does not require a planar interface. However, it still has problems as the temperature approaches the critical temperature, and is plagued with the statistical problems associated with using bins. Furthermore, as the temperature approaches the critical temperature, two distinct peaks in the distribution function may not be present so that the phase densities can not be extracted. The use of this method requires multiple parameters, which are provided as input into the procedure and may be functions of state point. Due to this functionality, the method must be calibrated to determine the optimum values of the parameters at each temperature.

In our previous work[13], we presented a method for the calculation of the two-phase envelope for MD simulations by Voronoi Tessellations (VT) using a simple Lennard-Jones fluid. VTs have wide applicability in various fields. One can use VT to determine the accessible volume of an adsorbent[52], determine the molar volume of a protein[15], study the physics of hard sphere fluids[42], and investigate crystal deformation[5]. There are various methods available for the calculation of the Voronoi Tessellation. See

the review by Aurenhammer[14] and the book by O'Rourk[16] for a good introduction to the various methods to create Voronoi diagrams.

In this work we have, for the first time, extended the use of VT in two-phase MD simulations to determine the coexisting densities of a polyatomic fluid, namely ethanol (C_2H_5OH). We compare our results to data from the literature for ethanol obtained by GEMC[20] and to a fit of experimental data[53], and determine coexisting densities, critical properties, vapor pressures, surface tensions, molecular orientation, and pair correlation functions along the two-phase envelope. Furthermore we address some of the issues of using VT to determine the phase densities.

4.2 Simulation Details

Two-phase MD simulations were performed to determine the VLE of explicit atom ethanol. The interaction potential utilized was the OPLS-AA of Jorgensen *et al.*[18], and the functional form of the OPLS-AA force field can be seen in equation (1) and the parameters used can be seen in Table 4.1.

$$U = \sum_{bonds} K_r \left(r - r_{eq}\right)^2 + \sum_{angles} K_\theta \left(\theta - \theta_{eq}\right)^2 +$$
$$\sum_{dihedrals} \frac{V_1}{2}\left[1 + \cos\left(\phi + f_1\right)\right] + \frac{V_2}{2}\left[1 - \cos\left(2\phi + f_2\right)\right] + \frac{V_3}{2}\left[1 + \cos\left(3\phi + f_3\right)\right] + \qquad (1)$$
$$\sum_i \sum_{j>i} 4\varepsilon_{ij}\left(\frac{\sigma_{ij}^{12}}{r_{ij}^{12}} - \frac{\sigma_{ij}^{6}}{r_{ij}^{6}}\right) + \frac{q_i q_j e^2}{r_{ij}}$$

The nonbonded interactions are calculated for all combinations of atoms on different molecules and for atoms separated by at least 3 bonds. The nonbonded interactions of molecules involved in tensional interactions (1, 4) are scaled by 0.5 for the Lennard-Jones and the electrostatic interactions.

When evaluating the electrostatic interactions in two-phase MD one has many different options. The most rigorous option is to utilize the Ewald summation[6,19] that would solve the electrostatic interactions exactly, but the use of the Ewald summation in an inhomogeneous system requires a great computational burden and can be prohibitive[19]. Reaction field is an additional option that utilizes a spherically truncated pair potential and a uniform dielectric constant. Although using reaction field[5] is computationally attractive, using a uniform dielectric constant to correct the electrostatic interactions in an inhomogeneous system would cause problems at the interface because the local environment is not uniform.

The Spherically Truncated Charge Neutralized (STCN) potential of Wolf *et al.*[19] was chosen as an acceptable compromise between accuracy and computational efficiency. The STCN potential utilizes a spherically truncated, charge neutralized potential that is functions of the local environment of the charge. Furthermore, relatively large cut-offs for the potential energy functions have to be used in two-phase MD to obtain the reasonable results for the bulk densities[12,33,36], so the effect of the correction is thought to be negligible.

The simulations were carried out on an in-house designed FORTRAN 90 code with MPI utilizing two time scale rRESPA[5,6,54,55]. The short time scale has a time step of

0.2 fs and contained all of the intramolecular interactions such as bond stretching, bond bending, bond torsion, and the nonbound intramolecular interactions. The larger time step was 2 fs and contained the Lennard-Jones and the electrostatic interactions. The temperature was also controlled in the larger time scale by a Nosé-Hoover thermostat[26,46].

The coexisting phases can be created in a MD simulation in three different ways. One can quench a vapor[10,11], expand a liquid[12], or place a slab of liquid in contact with a slab of vapor with initial guesses of the densities[7]. Although the procedure of quenching and expanding the simulation allows one to start with less information of the final condition of the system the time required for equilibration of the vapor and liquid phases can be prohibitive in large systems. To accelerate the equilibration of the phases we chose to place a slab of vapor in contact with a slab of liquid using initial guesses for the density.

The size of the liquid droplet was chosen such that it was larger than twice the cut-off distance of the interaction potentials. The vapor phase was chosen so that enough molecules were available for good statistics and the resulting unit cell was at least twice as large along the z axis as along the x and y axes to insure the proper interface orientation throughout the simulation. The minimum number of molecules was 2197.

Two different cut-offs were investigated. The smaller cut-off was 21 Å, which corresponds to the minimum value for Lennard-Jones systems of 6σ (using the largest σ of 3.5 for the carbon atoms)[12,33]. The second cut-off was 27 Å, the maximum value that could be used based upon the size of the smallest liquid droplet at 375 Kelvin, where we insisted that the size of the droplet be greater than twice the cut-off distance in all three

dimensions. The simulations with a cut-off of 21 Å were equilibrated for 2 ns before a 1 ns data production phase. The simulations using a cut-off of 27 Å started from the final configuration of the simulations with a cut-off of 21 Å. The simulations were equilibrated for an additional 0.2 ns followed by a data production of at least 0.4 ns.

4.3 Phase Determination

Using VT in a two-phase MD simulation uniquely divides the simulation cell into N (atoms or molecules) sub-regions. Each sub-region is uniquely defined by its nearest neighbors, the volume of every molecule (or atom), be it in the liquid, vapor, or interface. In order to apply these methods to molecular dynamics simulations, we chose to save the positions throughout the simulation and apply the method after the simulation has been completed due to its high computational burden. For both production sets 100 configurations were saved.

In terms of the numerical evaluation of the Voronoi volumes, there are several techniques employed to accelerate the calculation of the volumes. First, a sorted neighbor list is truncated to decrease the size of the inner loops in the calculation. Second, the procedure is implemented in parallel and the total number of molecules is divided among all the processors. When calculating the volumes of every molecule in an MD simulation, the calculation must be implemented with periodic images of the simulation cell. This insures that the Voronoi cell (the set of vertices around each molecule or atom) is closed or nondegenerate. The minimum image convention can be used in single-phase

simulations because the system is homogeneous. When calculating the volumes in a two-phase simulation, the minimum image convention may not be sufficient. If one imagines a very dilute gas, where only one or two molecules are in the vapor phase of a two-phase simulation then the vapor molecules would not have the minimum number of neighbors to close the Voronoi cell (at least 4 unique neighbors) or the resulting Voronoi cell would be shaped incorrectly and give an incorrect volume. When performing the tessellation in Euclidean space the average number of nearest neighbors is approximately 15.

In a two-phase simulation, the normalized variance of the individual volumes is used to determine the phases. We have outlined the procedure in our previous work on simple fluids [13]. In summary, one performs the Voronoi analysis on the two-phase system. To initiate the procedure, one selects initial guesses of the vapor and liquid densities. From a sorted list of Voronoi volumes, one identifies particles as liquid starting with the particle with the smallest Voronoi volume and continuing until one has the correct average liquid density. The variance of the Voronoi volume of that set is then computed. An independent single-phase simulation is performed at the temperature and estimated density. The variance of the Voronoi volume of the single-phase simulation is calculated and compared to that from the two-phase simulation. If they match, one has the correct density. If they do not match, one iterates with a new estimate of the density. Each iteration involves a small single-phase simulation. There is only one larger two-phase simulation. The procedure is also performed independently for the liquid and vapor phases.

Essentially, by identifying two parameters for each phase—the average Voronoi volume and the standard deviation of the Voronoi volume—we are able to guess one of the parameters and use the other one to self-consistently validate our guess, until it has converged. By coupling the phase determination to single-phase simulations the method removes all arbitrary choices and calibrations from the phase determination in molecular dynamics simulations. This procedure has been used to study the vapor-liquid equilibrium of a simple Lennard-Jones fluid [13].

In this work, we extend the procedure to a polyatomic fluid. When calculating the volumes of the individual molecules there are three different routes that can be taken. First, all the atoms on every molecule can be used for the Voronoi calculation. The resulting molecular volume would be the sum of the individual atomic volumes. Second, "pseudo-atoms", such as CH_2, CH_3 and OH in the case of ethanol, could be used to calculate the volume of each group, and then the groups could be summed to give the Voronoi volume. Finally, for small molecules the center of mass of each molecule could be used to give the Voronoi volume. The disadvantage of the most straightforward method, namely applying the Voronoi tessellation on atomic coordinates, is that the computational demands of the calculation is great and its poor scaling with number of particles. By using either pseudo-atoms or molecule center of mass, we can substantially reduce the computational requirement to a tractable amount. This method is the most computationally efficient, but can only be applied to small molecules. These methods are equivalent for small molecules because the VT is space filling. We provide a demonstration below.

4.4 Other Properties

Since two-phase MD simulations were performed, interfacial properties are also investigated. The surface tension, γ, was calculated throughout the simulation by the virial expression[7,34,50,56] for systems with planar interfaces. The expression can be seen in equation (2).

$$\gamma = \frac{1}{2A}\left\langle \sum_{i=1}^{N}\sum_{j>i}^{N}\left(1-\frac{3z_{ij}^2}{r_{ij}^2}\right) r_{ij}\frac{\partial u(r_{ij})}{\partial r_{ij}} \right\rangle \tag{2}$$

The symbols in equation 2 are as follows: γ is the surface tension; r_{ij} is the distance from atom i to atom j; z_{ij} is the z component of the distance from atom i to atom j; A is the surface area of the interface; $\partial u(r_{ij}) / \partial r_{ij}$ is the derivative of the potential energy. Equation (2) has been used widely to calculate the surface tension of many different systems, and it is equivalent[34] to the Irving and Kirkwood procedure to the calculation of the surface tension via its mechanical definition[33,56-59] for systems with planar interfaces shown by equation (3).

$$\gamma = \frac{1}{2}\int_{liquid}^{vapor}[p_N(z) - p_T(z)]dz \tag{3}$$

The symbols in equation (3) are as follows: γ is the surface tension; p_N is the normal component of the pressure tensor; p_T is the tangential component of the pressure tensor. Equation 2 is evaluated throughout the simulation spatially along the z-axis. There

is some ambiguity in the implementation of equation (3) because the virial has to be divided among bins along the z-axis. For this reason, we chose to use the virial expression shown in equation (2).

A long range correction must be applied to the surface tension to obtain the correct value. There are various formalisms for the long range correction in the literature, and we chose that of Chapela *et al.*[7] and Blokhuis *et al.*[60]. The functional form of the correction can be seen in equation (4).

$$\gamma_{tail} = 12\pi(\rho_{liq} - \rho_{gas})^2 \int_0^1 ds \int_{r_{cut}}^{\infty} drr^{-3}(3s^3 - s)\coth\left(\frac{2sr}{\xi}\right) \quad (4)$$

The interfacial thickness is denoted by ζ, ρ is the liquid and vapor density, and r_{cut} is the cutoff for the potential energy and is the lower limit of the second integral, *s* is the unit sphere coordinate and is integrated from 0 to 1.

Another interfacial property investigated is the molecular orientation. To determine the molecular orientation, a histogram was created to show the average angle spatially across the interface. The angle was determined from a vector defining the ethanol molecule ($\mathbf{v}_1$) and the vector normal to the planar interface ($\mathbf{v}_2$). The vector defining the ethanol molecule was the distance from the first carbon to the oxygen, as shown in Figure 4.1.

In addition to properties such as the surface tension and the molecular orientation, other properties were investigated along the two-phase envelope. These properties include the vapor pressure and the pair correlation functions (PCF) in the vapor and liquid phase and were determined from single-phase simulations at the saturated

densities. The single-phase simulations were performed with 512 molecules. The radial distribution functions were evaluated at two temperatures to determine the effect of hydrogen bonding as a function of temperature.

4.5 Results and Discussion

The first step to performing the Voronoi analysis was to determine if the centers of mass of the molecules could be used to determine the Voronoi volumes instead of all the atoms in the simulation cell. The test was performed by calculating the volumes via both routes to determine the distribution functions for the system. The resulting distribution functions of the molecular density (proportional to the inverse of the Voronoi volumes) can be seen in Figure 4.2 (a). The solid line is the distribution determined by calculating the Voronoi volume of every atom and summing to give the volume of each molecule. The markers are the direct calculations of the molecular volume from the center of mass of each molecule. The peaks for the liquid and vapor phases are at the same value, but the results for the all-atom method are slightly higher. In an attempt to visualize the differences in calculating the volume via the center of mass and all atom, a two dimensional tessellation was performed on a hypothetical system. The plot can be seen in Figure 4.2 (b). The small circles are representative of the pseudo-atoms, the center of mass is not shown. The solid black line represents the simulation box, the solid blue lines represent the tessellation performed on the “atoms” and the dashed red lines represent the tessellation performed on the centers of mass. The center of mass results do

not trace the exact same lines as the atomistic results, but the average "molecular" areas (in two dimensions) are equal and the sum of the individual areas equals the total area for each method.

The lines do not trace exactly the same curve for the "atomistic" and the "molecular" methods because of the differences in position of the center of mass and the position of the individual "atoms". This issue will become a problem for large molecules such as polymers, because the correct volume would not be obtained from the center-of-mass triangulation. This is not a problem for ethanol because there is very little difference between the center of mass of ethanol and the position of pseudo-atoms, as can be verified in Figure 4.2(a).

Based on these results, we choose to base our Voronoi tessellations on the center of mass of the molecules because it was more computationally efficient and gave essentially the same result as that based on the pseudo-atom approach. Of course, for longer chains, it would be necessary to use a Voronoi tessellation based on pseudo-atoms or true atoms.

In Figure 4.3 (a-c), we show the total distribution of the molecular density from the two-phase simulations at 375 K, 450 K, and 472 K respectively. At low temperature, there are two peaks corresponding to the liquid and vapor phases and an interfacial region between them. As the temperature increases, the peaks broaden and move closer to each other as the interfacial region begins to fill in.

Superimposed on the two-phase Voronoi distributions in Figure 4.3 are the molecular density distributions from the single-phase liquid and vapor simulations at the

converged densities. Also shown in these plots are the density distributions of the liquid and vapor phases from the two-phase simulation based on those molecules that were defined as liquid or vapor by our procedure. As we have seen with the simple system, the use of Voronoi volumes allows one to match closely the density distribution of the liquid phase in the two-phase simulation with that from the single-phase simulation, and likewise for the vapor. The key element to remember here is that, based on this procedure, two properties of the distribution, namely the mean value and the variance of the Voronoi volume, are identical for the single-phase liquid simulation and the liquid phase extracted from the two-phase molecular dynamics simulation (and analogously for the vapor). However, the shape of the distribution can be different. The agreement is not perfect, as was the case for the simple fluid. The discrepancy between distributions in the Voronoi volume for the vapor (or liquid) phase extracted from the two-phase simulations and generated by the single-phase simulation is attributed to the fact that the procedure used here is designed to converge on two features of the distribution—the mean and the variance. All higher order moments of the distribution are currently ignored. Essentially, there is an assumption that the distribution is completely characterized by the mean and the variance. Some distributions, such as a Gaussian distribution, are completely characterized by these two parameters. From the Voronoi distributions obtained from the single-phase simulations, we clearly see that the distributions are skewed (non-Gaussian), especially in the vapor phase at high temperature. Potentially, one could implement a convergence scheme that included higher-order moments of the Voronoi volume distribution to address this issue. We have not attempted that in this work. This

argument can at least partially explain why the agreement between the two-phase and single-phase simulations worsens as the temperature increases (because the distribution is skewed to a larger degree). It can also partially explain why the agreement was superior for the simple fluid [13] than for ethanol, in which the hydrogen bonding leads to this skewed distribution.

Using the VT also allows one to see the phases within the MD simulation volume. Figure 4.4(a–e) are snapshots of final configurations at all temperatures. The molecules are colored by their representative phase. The red molecules are in the vapor phase, the green molecules are in the liquid phase, and the blue molecules are in the interface. As was the case with simple fluids, using this unambiguous procedure generates a definition of the interface that is functions of temperature. At low temperature, where there exists a gap between the liquid and vapor density distributions, as shown in Figure 4.3(a-b), the interfacial molecules are neither liquid nor vapor. At higher temperatures, the liquid and vapor distributions overlap, such as in Figure 4.3(c), so that the interfacial molecules are both liquid and vapor. One consequence of using the Voronoi procedure to define self-consistently the liquid and vapor phases is that we observe some interfacial molecules dispersed in the "bulk" liquid and vapor phases, far from the interface.

The resulting two-phase envelope can be seen in Figure 4.5. This figure contains a fit of experimental data[53], simulation results generated by GEMC[20], and the results from this work for cut-offs of 21 Å and 27 Å. There is good agreement between the results from GEMC and the results from this work at a cut-off of 27 Å. The importance of interaction cut-offs to the width of a phase envelope has been previously studied[12,33,36].

We began with 21 Å because that had proven sufficient for the simple Lennard-Jones fluid. We found that we required a larger cut-off for ethanol to obtain results similar to GEMC. We believe that the large cut-off was necessary because our simulations were performed with the electrostatic interactions calculated via the STCN potential, and the electrostatic interactions for the GEMC were calculated by utilizing the Ewald Summation[6,19]. The averages and error bars for this work were calculated by determining the intersection of the single-phase and two-phase normalized variances for the liquid and vapor phases at every five configurations. The error bars represent one standard deviation, and the data with uncertainties are displayed in Table 4.2.

The critical properties for our work are 483 K, 270 kg/m^3, and 7.9 MPa. These were determined by fitting the Ising scaling for the critical temperature, the line of rectilinear diameter for the critical density, and using the Antoine Equation for the critical pressure. The resulting errors are -6% for the critical temperature, -3% for the critical density, and 30% for the critical pressure as compared to the experimental data (T_c = 513.09 K, ρ_c = 276.01 kg/m^3, and P_c = 6.148 MPa)[53]. There is a difference between our value for the critical temperature and the value reported in the literature[20] for the OPLS-AA potential (T_c = 508 K). We attribute this difference to the fact that, using the Voronoi procedure, we are able to obtain the phase diagram closer to the critical point (up to 472 K), whereas the work from the literature reported values up to 455 K[20].

Figure 4.6 shows the resulting surface tension as functions of temperature. The markers are the results from this work and the solid line is the fit from the Chemical Properties Handbook by Yaws [61]. As expected, the surface tension decreases with

increasing temperature to a value of zero at the critical temperature. Included in the surface tension is the long-range correction shown in equation (4). The interface thickness was determined from the widths of the peaks generated from the spatial histograms of molecular orientation shown below. Since there was no longer a planar interface present at a temperature of 472 Kelvin, the surface tension is not reported, since the determination of interfacial thickness relies on a planar interface[34]. (Note that our procedure for the determination of the phase diagram and critical properties does not require a planar interface.) The average error between our simulated surface tension and the prediction of the experimental surface tension[61] was 60%. The long-range correction to the surface tension accounted for less than 0.25% of the final value. The error bars shown in Figure 4.6 represent one standard error, and the simulation results can be seen in Table 4.2.

Spatial histograms of the molecular orientation can be seen in Figure 4.7. These are shown for two temperatures, 375 K (a) and the 450 K (b). As can be seen in Figure 4.7, there is a preferential orientation of the molecules at the interface. The range of the angle shown in Figure 4.1 is 0° to 180°, so that the average is 90° in an isotropic system. In the bulk liquid and bulk vapor, the average value of the orientation angle is indeed 90°. At each interface in our periodic system, there is deviation from the bulk value, corresponding to a systematic orientation of the ethanol molecules, such that the alcohol group is closest to the liquid droplet. This orientation maximizes the hydrogen bonding of the interfacial ethanol with the dense liquid phase. As temperature increases, we observe less orientation, indicating that this preferential orientation is indeed energetic in nature.

From the spatial histograms of molecular orientation, the interface thickness was determined. The resulting interface thickness in Å is shown in Figure 4.8 as functions of temperature. The interface increases in width until it cannot be distinguished from the liquid and vapor phases.

To investigate further the hydrogen bonding within the phases, pair correlation functions (PCFs) were calculated for the vapor and liquid phases. The PCFs were determined from single-phase simulations on the two-phase envelope at 375 K and at 450 K. The resulting distribution functions can be seen in Figure 4.9. The PCFs were determined for the interactions of the oxygen from the alcohol group (i) to other oxygen, (ii) to the hydrogen on the alcohol group, and (iii) to all hydrogen in the simulation volume. In both phases, the first peak in the O-H_{OH} PCF corresponds to a hydrogen bond. The first peak in the O-O PCF corresponds to the fact that the H atom involved in the hydrogen bond is also chemically bound to an O atom. The second peak in the O-H_{OH} PCF corresponds to an H atom that is hydrogen bound to the O-atom in the first peak of the O-O PCF. There is relatively little hydrogen bonding between the O atoms and the H atoms chemically bound to C atoms.

Significant hydrogen bonding can be seen in all of the PCFs, including the vapor phase. The appearance of hydrogen bonding in the vapor phase for ethanol is not a new observation; in fact it has been shown by experimental results[62,63], molecular dynamics simulations[64], and by quantum simulations[65]. The PCFs show that it is energetically favorable for the ethanol molecules in the vapor phase to share a hydrogen bond with other ethanol molecules.

The vapor pressure is shown in Figure 4.10 and in Table 4.2. There is considerable disagreement between the experimental fit[66,4] and the simulation data. The simulated vapor pressure is always too high, relative to the experimental data. We believe that this and the other discrepancies between the simulation results and experimental data is largely due to limitations of the potential used in this work and should not be attributed to uncertainties in the phase diagram resulting from the Voronoi procedure. The Voronoi procedure delivered excellent results for the simple Lennard-Jones fluid, compared to methane experimental results, where the potential is very reasonable. We do acknowledge that the Voronoi distribution of the vapor phase from the single-phase simulation is strongly skewed, with a long tail to high density near the critical temperature. This skew of the probability distribution is not captured by matching only the mean and variance of the Voronoi distributions. This issue can be resolved in the future by using a more sophisticated potential for ethanol and coupling it to the Voronoi procedure.

4.6 Conclusions

Voronoi Tessellations have been coupled with two-phase molecular dynamics simulations to determine the vapor-liquid phase diagram of ethanol near the critical point. This demonstrates that the Voronoi procedure outlined in previous work[13] is equally applicable to polyatomic systems. The coexisting densities agree well with values reported in the literature from GEMC[20] at low temperatures, where they are available.

We are able, using the Voronoi approach, to generate coexisting densities much closer to the critical point than standard methods available in the literature for direct simulation of phase equilibria. The critical properties from this work deviated from experimental values by -6%, -2% and 30% for the temperature, density, and pressure respectively. The surface tension was determined up to a temperature of 450 Kelvin and deviated from experimental data [61] by 60%. At the interface, ethanol molecules prefer to have their alcohol group oriented toward the liquid phase, in order to maximize hydrogen bonding. From the pair correlation functions, we observed significant hydrogen bonding in the liquid and vapor phase.

4.7 Acknowledgements

The authors gratefully acknowledge the financial support of the Office of Fossil Energy of the U.S. Department of Energy (DOE). Through the UT Computational Science Initiative, this research project used resources of the Center for Computational Sciences at Oak Ridge National Laboratory, which is supported by the Office of Science of the DOE under Contract DE-AC05-00OR22725.

Appendix A: Figures and Tables

Table 4.1: Parameters from the OPLS-AA potential[18] for this simulation study to represent ethanol.

Atom	σ(Å)	ε(kcal/mol)	q(e^-)
H, RH	2.5	0.03	0.06
C, RCH_3	3.5	0.066	-0.18
C, CH_3OH and RCH_2OH	3.5	0.066	0.145
H, ROH	0	0	0.418
O, ROH	3.12	0.17	-0.683

Bond Stretching	k_r (kcal/(mol*Å^2))	r_{eq} (Å)
C-C	268	1.529
C-H	340	1.09
C-O	320	1.41
O-H	553	0.945

Bond Bending	k_θ (kcal/(mol*rad^2))	θ_{eq} (deg)
H-C-C	37.5	110.7
C-C-O	50	109.5
H-C-H	33	107.8
H-C-O	35	109.5
C-O-H	35	109.5

Bond Torsion	V_1 (kcal/mol)	V_2 (kcal/mol)	V_3 (kcal/mol)
H-C-C-O	0	0	0.468
H-C-C-H	0	0	0.318
C-C-O-H	-0.356	-0.174	0.492
H-C-O-H	0	0	0.45

Table 4.2: Results from this work for the liquid density (ρ_L), vapor density (ρ_V), vapor pressure (P_{vap}), and surface tension (γ) as functions of temperature. The subscripted number is the uncertainty in the last digit.

Simulation Results				
T (K)	ρ_L(kg/m^3)	ρ_V(kg/m^3)	P_{vap} (MPa)	γ (N/m)
375	693_5	6.6_7	0.41_1	0.025_6
400	655_4	15_3	0.91_3	0.021_4
425	603_2	30_8	1.84_4	0.013_4
450	551_7	57_4	3.6_1	0.008_2
472	419_7	125_{19}	6.2_2	

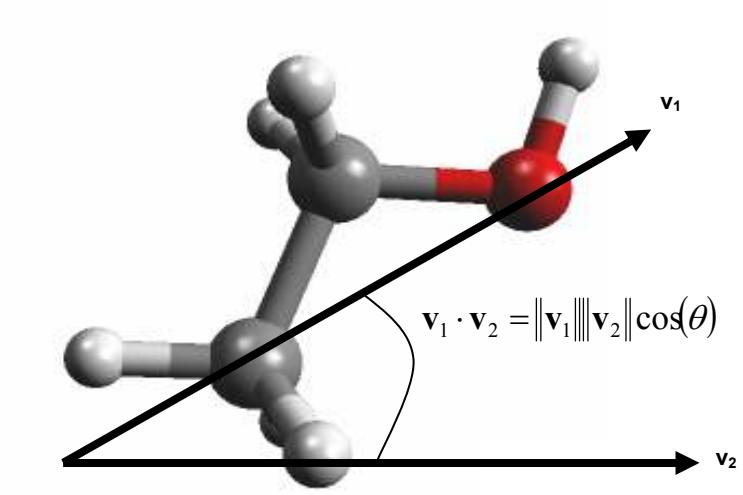

Figure 4.1: Illustration of how the angle was calculated for each molecule. $\mathbf{V}_1$ is the vector describing the distance from the carbon in CH3 to the oxygen in OH, and $\mathbf{V}_2$ is the vector normal to the planar interface.

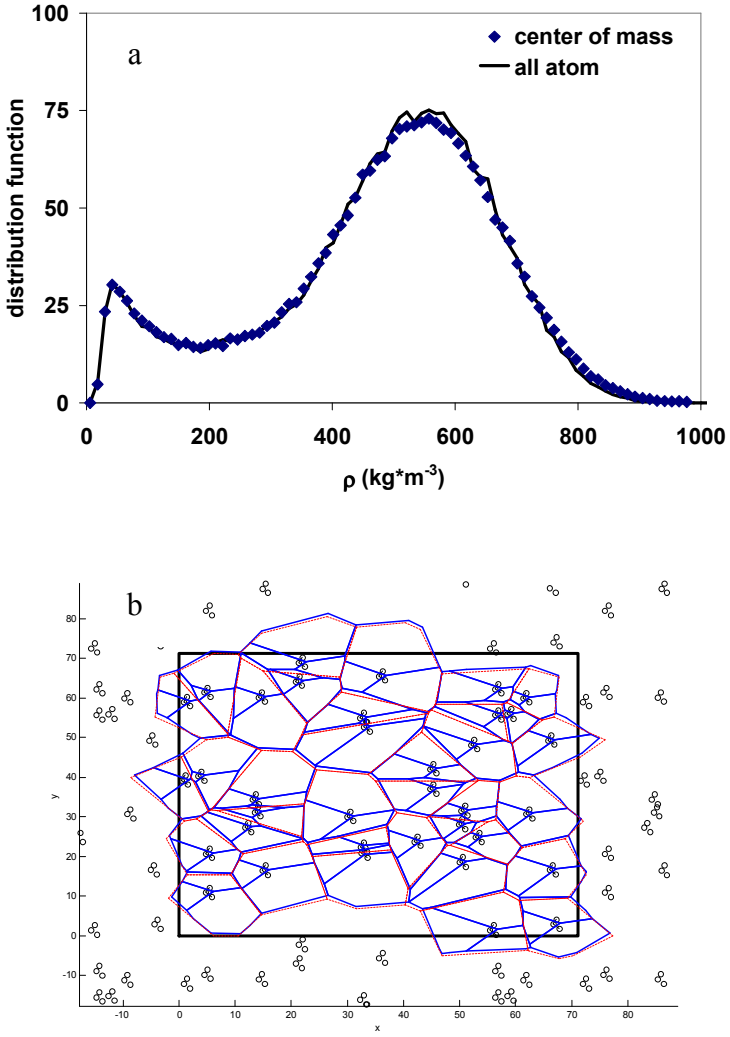

Figure 4.2: (a) Density distribution functions for a two-phase simulation at 450 K. The squares represent the volumes calculated from the molecules center of mass, and the dashed line represents the volumes calculated from every atom in the simulation volume. (b) Center of mass tessellation compared to an all atom tessellation for a hypothetical two dimensional case.

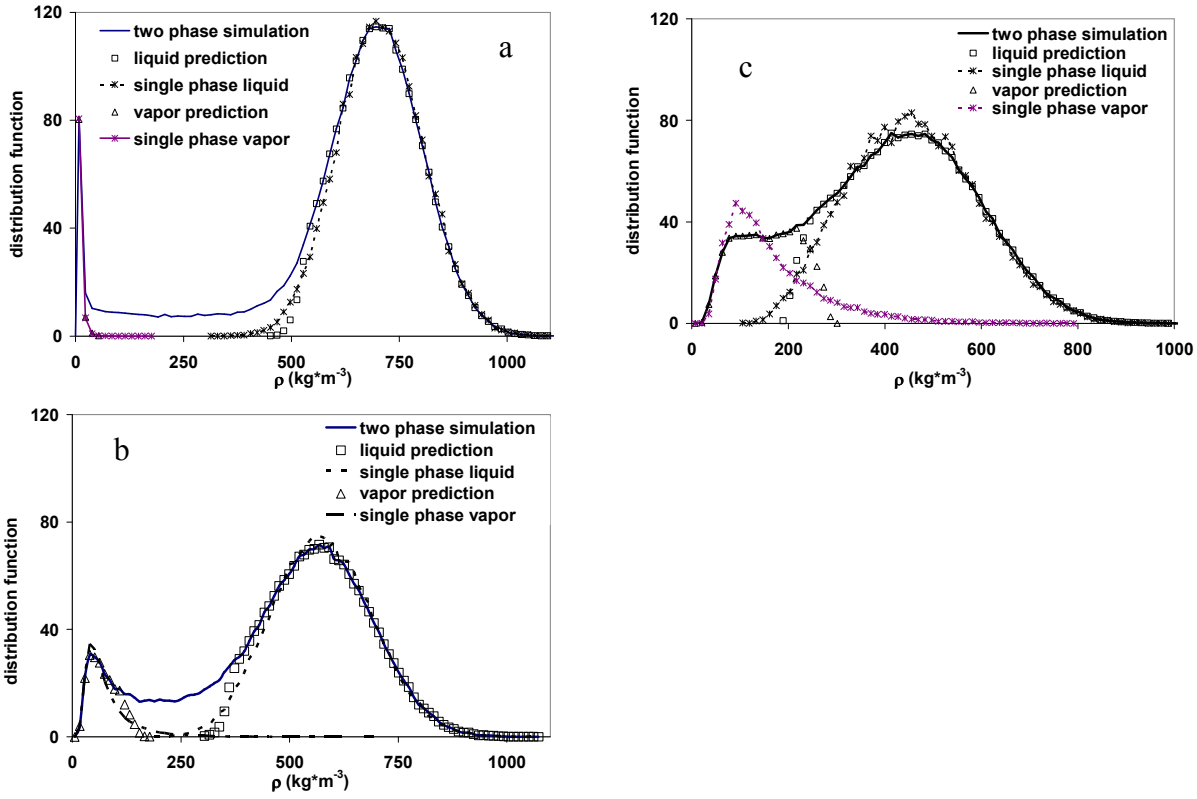

Figure 4.3: Density distribution functions for the two-phase simulations. The squares and the triangles are the predictions from our method for the liquid and vapor phases respectively, the solid line is the distribution of the two-phase simulation, and the dashed lines are the distribution from single-phase simulations for (a) 375 K and (b) 450 K.

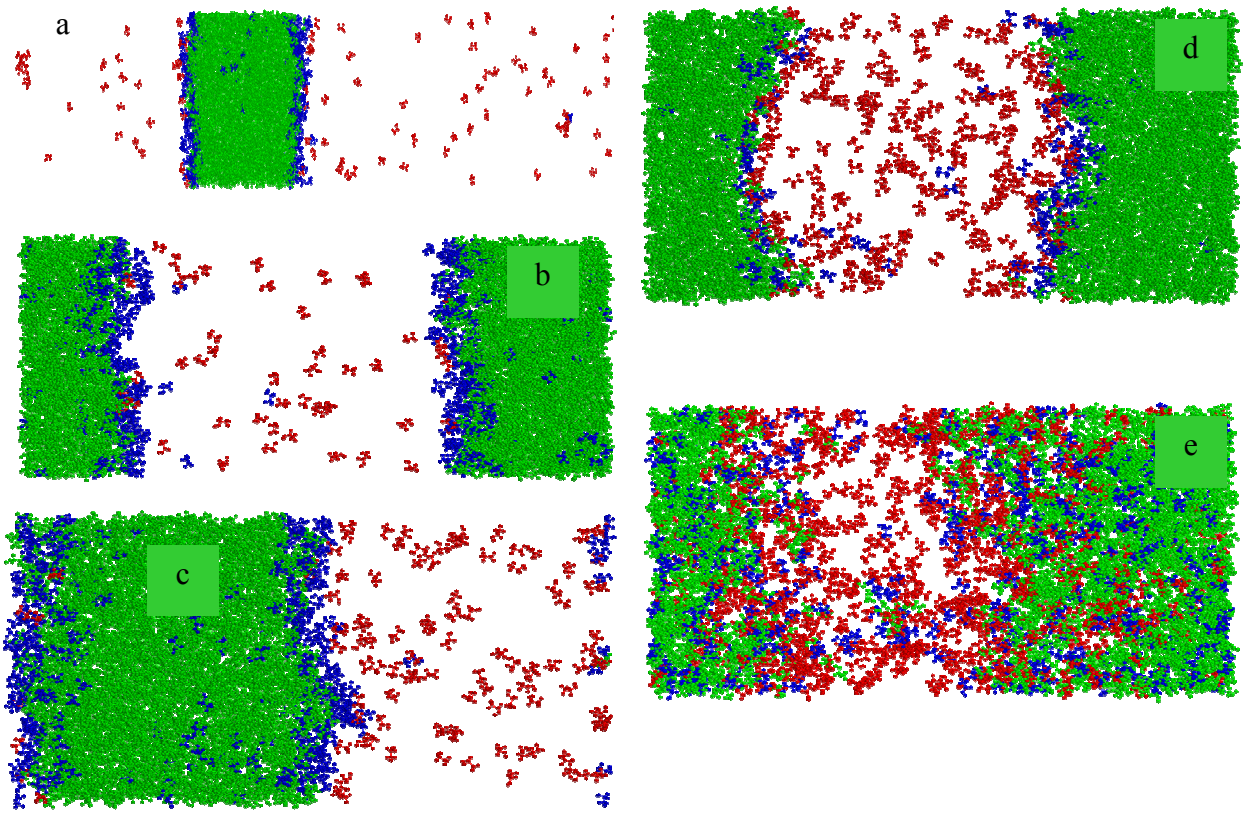

Figure 4.4: Snapshots of final configurations for the two-phase simulation. The following convention has been used to label the molecules: liquid is green, vapor is red, and interfacial is blue for (a) 375 K, (b) 400 K, (c) 425 K, (d) 450 K and (e) 472 K.

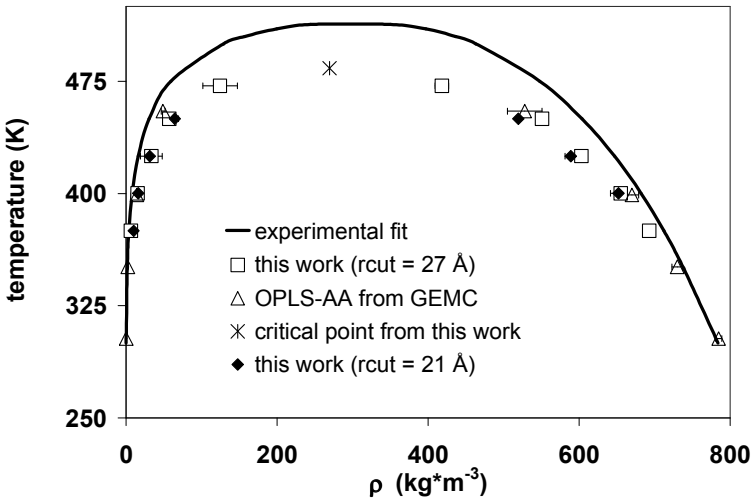

Figure 4.5: Vapor-liquid phase diagram for ethanol. The line is an experimental fit[53], the squares are results from this work with a potential cut-off of 27 Å, the triangles are published results from GEMC[20], the Xs are the results from this work with a potential cut-off of 21 Å, and the asterisk is the critical point from this work.

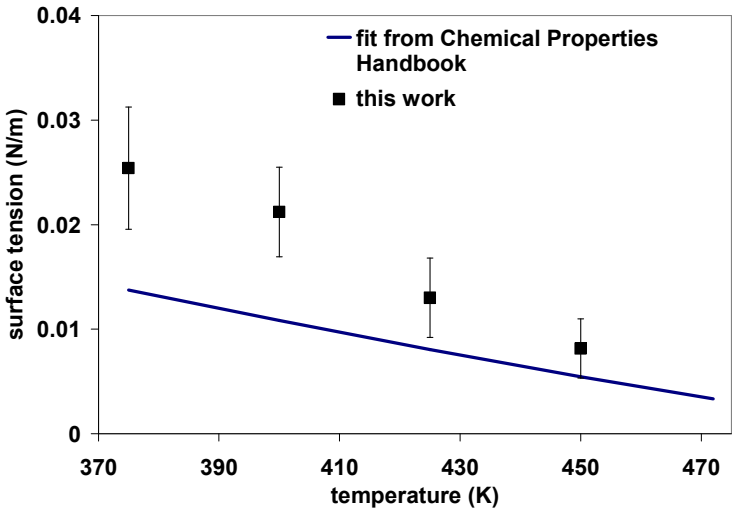

Figure 4.6: The surface tension (N/m) of ethanol as functions of temperature (K). The solid line is a fit from the Chemical Properties Handbook[61].

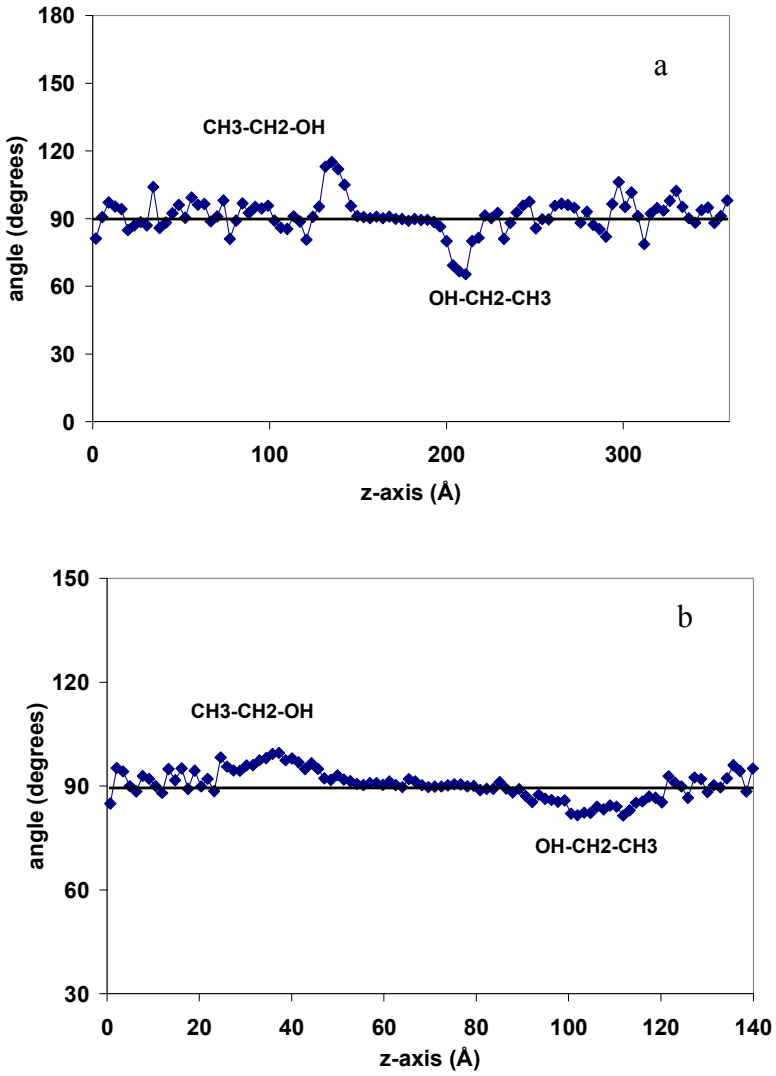

Figure 4.7: Spatial histogram of average molecular angle within the simulation cell at two temperatures (a) 375 K, and (b) 450 K.

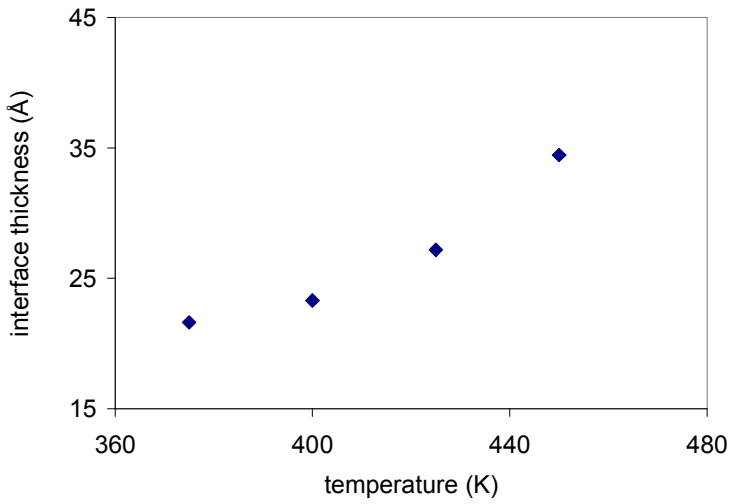

Figure 4.8: Interface thickness from the angle distribution within the simulation cell.

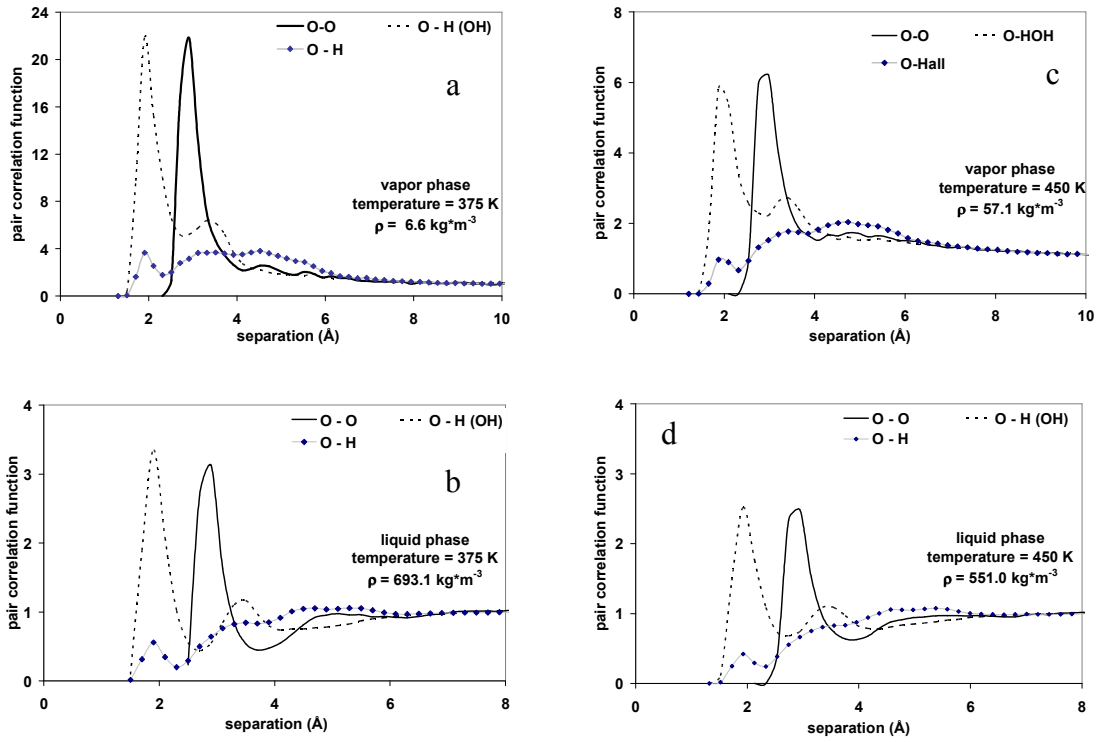

Figure 4.9: Pair correlation functions for the (a) vapor phase at 375 K, (b) liquid phase at 375 K, (c) vapor phase at 450 K, and (d) liquid phase at 450 K. The solid line is the distribution of the oxygen to other oxygen, the dashed line is the distribution of oxygen with only hydrogen from an alcohol group, and the line with markers is the distribution of oxygen with all hydrogen.

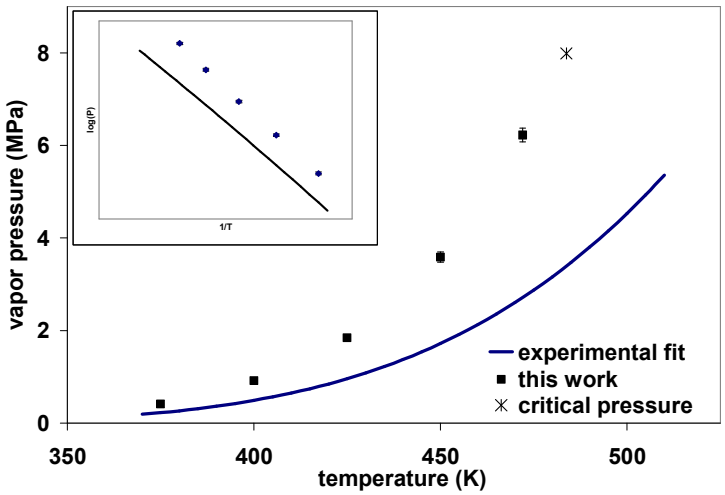

Figure 4.10: Vapor pressure of ethanol. Squares represent results from this work and the solid line is a fit of experimental data[66,67]. The inset plot is the vapor pressure data for log (P) vs. 1/T.

CHAPTER 5

Vapor-Liquid Equilibrium of Ethanediol by Molecular Dynamics Simulation and Voronoi Tessellation

Abstract
In this chapter, ethanediol is simulated using the TraPPE-UA force field. The force field was modified to include bond stretching modes. The stretching modes were determined by performing *ab initio* calculations to scan the potential energy surface. The Voronoi Method was applied to determine the vapor and liquid densities along the phase envelope. The results are compared to published literature values from GEMC, and there is some disagreement between the results presented in this chapter and the literature values. The densities from this work are always too low on the vapor side and too high on the liquid side. This discrepancy is attributed to the modification of the potential. The extrapolated critical temperature from this work is 728 K and direct simulations were performed at a temperature of 725 K. The surface tension was also calculated and there is excellent agreement between the simulated results and the experimental results.

5.1 Introduction

Ethanediol is a compound for which there is still much left unknown. Its thermal instability and high values of it critical properties make it difficult to measure accurately many of its properties[68]. This is evident by the many different values available for the critical temperature. The NIST Chemistry Webbook [67] reports five values for the critical temperature. The minimum value reported is 645 K and the maximum value is reported at 790 K; the only value that is repeated is 720 K. Accurate predictions of the critical properties are essential to chemical engineers. Using corresponding states approximations these properties can be used to predict how a compound will behave at a given temperature, pressure, and density.

For thermally unstable compounds such as ethanediol, molecular simulation can lead to accurate prediction of the thermophysical properties. The most widely used simulation technique to measure vapor-liquid equilibrium is Gibbs Ensemble Monte Carlo (GEMC)[6,12,69]. GEMC simulates a bulk vapor and a bulk liquid in separate simulation cells. The individual cells are allowed to swap particles and change volumes

all while maintaining a constant chemical potential, pressure, and temperature. Problems arise with GEMC as the temperature approaches the critical temperature. Close to the critical temperature the identities of the individual simulation cells can swap, smearing out the data [6]. Once this swap occurs, one utilizes an indirect simulation technique such as Histogram Reweighting or Gibbs-Duhem integration to determine the remainder of the phase envelope[6].

Other techniques available to study phase equilibrium are the NPT + test particle method[37], the Grand Equilibrium method of Vrabec[70] and Molecular Dynamics (MD)[7,10,13,17,33,36,71]. MD is different than these other methods because the simulation of the vapor and the liquid is performed in the same (single) simulation cell. Having both phases in the simulation cell creates an interface within the volume. The interface allows the investigation of properties not available to the other methods, for example, the surface tension.

Although the presence of an explicit interface being present allows for the investigation of new and interesting properties, it causes difficulties extracting the densities of each phase. Past methods utilized to determine the phase densities include the use of an empirical hyperbolic tangent function[7,33,36,71], and utilizing spatial and inverse histograms[10,11]. These methods fail as the temperature approaches the critical temperature, and have too many adjustable parameters. These adjustable parameters force one to calibrate the histogram methods before they could be used accurately in a two-phase system. The calibration has to be performed at every temperature because the optimum bin size may be functions of state point.

These deficiencies in the phase density extraction motivated us to develop the Voronoi method (VM)[13,17] to determine the densities. The VM has been successfully applied to both simple fluids and polyatomic fluids. The VM utilizes Voronoi tessellations[14-16] to determine the volume of every molecule within the simulation cell. This method couples the molecular volume of single-phase simulations to the molecular volume of two-phase simulations through simple statistical parameters such as the mean and variance.

The scope of this work is to (1) determine the phase envelope for ethanediol using MD and our Voronoi method; (2) determine the critical parameters of ethanediol; (3) measure the surface tension as functions of temperature; (3) measure the vapor pressure; (4) investigate hydrogen bonding along the phase envelope; (5) measure the affect of adding degrees of freedom to an accepted potential from the literature on the thermophysical properties.

5.2 Simulation Technique

The Transferable Potentials for Phase Equilibria (TraPPE-UA) force field[69] was chosen as the best candidate to represent ethanediol because it has been explicitly parameterized for diols (including ethanediol), and it was recommended in the literature as being the most reliable potential for measuring phase equilibria[20]. The TraPPE-UA force field utilizes United Atoms (UA) to represent the atoms within a molecule. The

hydroxyl hydrogen and oxygen are represented explicitly and the hydrogens attached to carbon atoms are merged into one sphere. The resulting change in the ethanediol structure is shown in Figure 5.1. The typical formalism for the TraPPE-UA is to use fixed bond distances, harmonic oscillators for the bond bending, and a cosine series for the torsions. The non-bound interactions utilize a Lennard-Jones potential and partial charge for the electrostatic interactions. The functional form of the force field can be seen in equation (1). The parameters used in this study are shown in Table 5.1.

$$
\begin{aligned}
U(r_{ij}) &= u_{bend} + u_{tors} + u_{repulsive} + u_{LJ} + u_{ES} \\
u_{bend} &= \frac{k_\theta}{2}(\theta - \theta_{eq})^2 \\
u_{tors} &= c_0 + c_1[1+\cos(\phi)] + c_2[1+\cos(2\phi)] + c_3[1+\cos(3\phi)] \\
u_{repulsive} &= \frac{a_{ij}}{r_{ij}^{12}} \\
u_{LJ} &= 4\varepsilon_{ij}\left[\left(\frac{\sigma_{ij}}{r_{ij}}\right)^{12} - \left(\frac{\sigma_{ij}}{r_{ij}}\right)^{6}\right] \\
u_{ES} &= \frac{q_i q_j}{4\pi\varepsilon_0 r_{ij}}
\end{aligned}
\qquad (1)
$$

In equation (1) the U(rij) is the total energy and the u represents the individual components of the total energy. The non-bound interactions include interactions of atoms separated by more than 3 bonds (1-4 interactions).

As mentioned above, the TraPP-UA force field utilizes fixed bond distances when employed in Gibbs Ensemble Monte Carlo (GEMC) simulations. We chose to fit the

bond stretching modes of ethanediol by utilizing Gaussian 98 [21] to scan the potential energy surface at the B3LYP/6-31G* level of theory. This model chemistry and level of theory has been shown to accurately reproduce vibration frequencies of organic molecules[72,73]. Equation (2) shows the functional form of the fit for the bond stretching energy. The resulting parameters are presented in Table 5.2. Also shown in Table 5.2 are the accepted bond distances from the TraPPE-UA potential.

$$u_{str} = \frac{k_s}{2}\left(r_{ij} - r_{eq}\right)^2 \tag{2}$$

$$U\left(r_{ij}\right) = u_{str} + u_{bend} + u_{tors} + u_{repulsive} + u_{LJ} + u_{ES} \tag{3}$$

The resulting total potential energy is shown in equation (3).

The electrostatic interactions were calculated utilizing the Spherically Truncated, Charge Neutralized potential (STCN) of Wolf and coworkers[19]. Although the method of choice is the Ewald summation[5,6,19], since it can calculate the electrostatic interactions exactly. It can be prohibitive for large inhomogeneous systems. The STCN potential was chosen as a compromise between computational efficiency and accuracy.

The simulations were performed using an in-house designed FORTRAN 90 code with MPI and two time scale rRESPA[5,6,54,55]. The intramolecular interactions were calculated at the short time step (0.2 fs). The longer time scale was 2 fs and contained all the Lennard-Jones and the electrostatic interactions. The temperature was also controlled at the longer time scale by a Nosé-Hoover thermostat[26,46].

To perform a two-phase simulation by Molecular Dynamics (MD), one can quench a vapor[10,11], expand a liquid[12], or place a slab of vapor in contact with a slab of liquid[7,33,36,71]. We chose to place a slab of vapor in contact with a slab of liquid at initial estimates for the density and allowed the phases and the interface to equilibrate. Although this method requires one to estimate the phase densities, it is by far the most computationally efficient way to obtain a two-phase system.

The initial simulation volume was a paralleliped with the z-axis being at least 2.5 times larger than the x and y axes. The size of the initial liquid droplet controlled the x and y axes, and the size of the initial vapor phase controlled the size of the z axis. This geometry forces the interface to be planar (at low temperatures) in the z axis. The minimum total number of molecules used in this simulation study was 3500. The simulation geometry was constructed such that each phase was larger than twice the cut-off distance for the nonbound potential energy functions.

The cut-off distance for the nonbound interactions was 25 Å for all simulations. This cut-off was verified by evaluating the total potential energy for different values of the cut-off for 4 two-phase systems. The results can be seen in Figure 5.2; the potential energy is constant for any cut-off larger than 14 Å within the two-phase system for temperatures 500, 550, 600, and 650 K.

To measure the phase densities along the phase envelope, we utilized the Voronoi method to determine the volume of every molecule in the simulation cell. By measuring the volume of every molecule and utilizing simple statistical parameters, such as the mean and variance, one can unambiguously determine the phases in a two-phase

simulation. In an earlier works by this group, this method has been applied to simple Lennard-Jones fluids[13] and to polyatomic fluids[17]. In addition to the two phase envelope, the surface tension, the vapor pressure, and hydrogen bonding were also investigated in this work.

5.3 Results and Discussion

By using the Voronoi method, we can determine the distributions of the molecular volume within the simulation cell. The resulting normalized distributions of the molecular densities (density is equal to 1/molecular volume) can be seen in Figure 5.3. As one can see from the figure at low temperatures there are two independent phases present in the simulation cell. As the temperature increases, the peaks corresponding to the vapor and liquid phases move closer together and the molecules which constitute the interface increase.

The Voronoi method allows determination of the phase densities from simple statistical parameters from both the two-phase and single-phase simulations. Figure 5.4 (a-c) shows the resulting phases within the simulation cell. In the figure, the liquid molecules have been colored green, the vapor molecules have been colored red, and the interface molecules are blue. One can see from Figure 5.4 that at lower temperatures the interface molecules are primarily located at the bulk interface. As the temperature increases, the interface molecules begin to appear in the bulk liquid and vapor phases.

In addition to being able to visualize the phases within the simulation cell, one can view the comparison of the single-phase and the two-phase density distributions. The single-phase density distributions were determined by performing small simulations at the density predicted by the VM. The comparisons for temperatures of 600 K and 700 K are shown in Figure 5.5 (a-b). For more discussion on the comparison of the distributions, please see our previous work[17].

The resulting phase envelope is shown in Figure 5.6. The results from this work are represented by solid grey markers; the published results [69] from GEMC are represented by blue diamonds. For many cases, the error bars are smaller than the marker. As can be seen in Figure 5.6, there is a discrepancy between the results reported by GCMC and our work. The discrepancy is caused by the inclusion of the bond stretching parameters without any modification of any of the other parameters in the TraPPE-UA potential. The density on the liquid side of the phase envelope is always too high and the density of the vapor side is always too low. Therefore, the addition of the shorter bond lengths and harmonic oscillators for the stretching modes caused the phase envelope for ethanediol to increase in breadth. Since the width of the phase diagram has increased, the critical temperature is higher than the reported value from GEMC.

The critical properties were determined by fitting the line of rectilinear diameters for the critical density, and fitting the Ising scaling law to determine the critical temperature[6,34,35]. Equation (4) shows the equation for the line of rectilinear diameter; equation (5) shows the Ising scaling law:

$$\overline{\rho} = \rho_c + A(T - T_c) \quad (4)$$

$$\Delta\rho = B(T_c - T)^{\beta} \quad (5)$$

The exponent for the scaling law is fixed to the classical value of 0.32. The resulting critical temperature is 728 K and the critical density is 0.338 g/cm^3. The critical temperature is above the value from GEMC[69] of 718 K and the experimental value of 720 K [67]. The critical density agrees well with the value from GEMC (0.340 g/cm^3) [69].

To determine the surface tension, the virial expression[17,35,50] was used throughout each two-phase simulation. By using the virial expression throughout the simulation, we are able to calculate the mean and standard error in the traditional manner without using any complicated integrations. The virial expression has been shown to be equivalent[35] to the Irving and Kirkwood formalism used to determine the surface tension by integrating the normal and tangential components of the pressure tensor[33,56,57,71].

The resulting surface tension is shown in Figure 5.7. As expected the surface tension decreases to zero at the critical temperature. As mentioned before the error bars represent one standard error as calculated throughout the simulation. There were two sets of data for experimental measurements of surface tension of pure ethanediol[74,75]. There appears to be a disagreement between the two sets of experimental data. Our simulation work matches best with the work of Hoke and Chen as can be seen in Figure 5.7. The results from this work are denoted with squares.

The vapor pressures were determined from independent vapor phase simulations at the vapor density determined by the VM. The vapor pressure results are shown in Figure 5.8. The vapor pressure from this work is marked by the yellow triangles, the

published results from GEMC[69] are the asterisks, and experimental data[66] from the literature are represented by the solid line. Once again, we see that the addition of the bond stretching parameters affected the results. The vapor pressure is lower than the results from the GCMC simulations. This is due to an additional term added to the virial expression that was not present in the initial parameterization. It is assumed that the non-bound interactions were fit to match the experimental values for the vapor pressure, and the addition of the bond stretching term has shifted the results.

Table5.3 reports the vapor densities, the liquid densities, the vapor pressure, the surface tension, and the critical properties determined from this work. The subscript in the table represents one standard error in the property.

To investigate hydrogen bonding along the phase envelope, single-phase liquid simulations were performed at the phase densities determined. Vapor phase hydrogen bonding analysis was also performed, but the results are not reported here. Each ethanediol molecule has at most four intermolecular hydrogen bonding sites (assuming only one bond site), so every site on each molecule was checked for a hydrogen bond for a series of hydrogen bond cut-off distances. Then clusters of hydrogen bonds were formed from the lists thus created. Figure 5.9 (a-c) shows the results from this analysis at three different temperatures and densities for single-phase liquid simulations. The plots are for (a) the average number of hydrogen bonds per molecule, (b) the average cluster size, and (c) the average maximum cluster size at each configuration. This analysis is different from other work in the literature[69] because we investigated the hydrogen bond

network for multiple cut-offs and determined the total size of the hydrogen bonded clusters.

There are many interesting features to these plots. Figure 5.9 (a) shows the average numbers of hydrogen bonds as functions of cut-off distance. For all cut-offs larger than 5.5 Å, all four of the hydrogen bonds are being utilized. As the temperature increases and the density decreases this location of the asymptote remains the same, but the rate at which the average number of hydrogen bonds changes drastically as functions of cut-off distance. Figure 5.9 (b) is the average chain length as functions of hydrogen bond distance. For this analysis, 216 molecules were used in the simulation, so the maximum cluster size is 216. For any cut-off larger than 2.75 Å, the size of the cluster rapidly increases. There appears to be a point of inflection in each of the data sets between 3.75 and 4.0 Å. As the temperature increases and the density decreases, the maximum value also decreases. So the appearance of smaller clusters becomes more probable. Figure 5.9 (c) shows the average maximum cluster size within the simulation cell. At lower temperatures and higher densities, the maximum cluster size is essentially the total numbers of molecules for any hydrogen bond distance greater than 4.0 Å. At 700 K, the average maximum cluster size is essentially constant for distances larger than 4.5Å. For 500 and 600 K, the average maximum cluster size is constant for any distance larger than 3.5Å. As the distance decreases from these points, the average maximum cluster size rapidly decreases to one. The results for 700 K do not decrease as rapidly as the results from 500 and 600 K. This suggests that at 700K the system is broken down into smaller hydrogen bonded clusters than at lower temperatures.

5.4 Conclusions

The VLE of ethanediol was determined from MD and the Voronoi Method. The phase envelope was extended well beyond the literature values to 725 K. From the phase envelope, we were able to obtain a critical temperature of 730 K and a critical density of 0.338. The effect of adding bond stretching modes to a potential was also investigated. It is found that any adjustment to the original parameters can affect the results. The bulk of the discrepancies arose in the liquid phase where the shorter bond distances and harmonic oscillators for the forces caused the molecules to pack tighter.

Other properties we investigated were the surface tension and the vapor pressure. The surface tension is in excellent agreement with the results of Hoke and Chen [74], and the vapor pressure results compare well with the published results from GCMC[69] and experimental data[66]. The results are slightly lower than those from GCMC[69] due to the additional bond stretching term included in the virial that was not in the original parameterization.

Hydrogen bonding on the phase envelope was also investigated. We determined the average number of hydrogen bonds per molecule as functions of cut-off distance, temperature, and density. The average hydrogen bonded cluster size and the average maximum hydrogen bond cluster size were also determined as functions of temperature and density.

5.5 Acknowledgements

The authors gratefully acknowledge the financial support of the Office of Fossil Energy of the U.S. Department of Energy (DOE). Through the UT Computational Science Initiative, this research project used resources of the Center for Computational Sciences at Oak Ridge National Laboratory, which is supported by the Office of Science of the DOE under Contract DE-AC05-00OR22725.

Appendix A: Figures and Tables

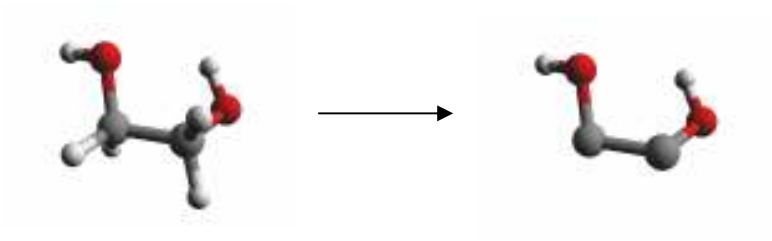

Figure 5.1: Comparison of explicit atom ethanediol and united atom ethanediol.

Table 5.1: Potential Parameters for the TraPPE-UA potential for ethanediol used in this study.

Non Bound	ε (K)	σ (Å^3)	q (e)	
CH2	46.000	3.950	0.265	
O (OH)	93.000	3.020	-0.700	
H (OH)	0.000	0.000	0.435	
Bend	k_θ (kcal/mol*rad^2)	θ (deg)		
C-C-O	99.954	112.000		
C-O-H	110.089	108.500		
Torsion	c_0 (kcal/mol)	c_1 (kcal/mol)	c_2 (kcal/mol)	c_3 (kcal/mol)
C-C-O-H	0.000	0.417	-0.058	0.373
O-C-C-O	1.000	0.000	-0.500	2.000
Repulsion	a_{ij} (K Å^{12})			
H(OH)-H(OH)	7.500E+07			

Table5.2 Bond stretching parameters used in this work and the accepted bond lengths for the TraPPE-UA force field.

	B3LYP/6-31G*		TraPPE-UA
Type	k_s (kcal/mol*Å^2)	req (Å)	req(Å)
C-C	640.844	1.520	1.54
C-O	828.410	1.417	1.43
O-H	1008.721	0.968	0.945

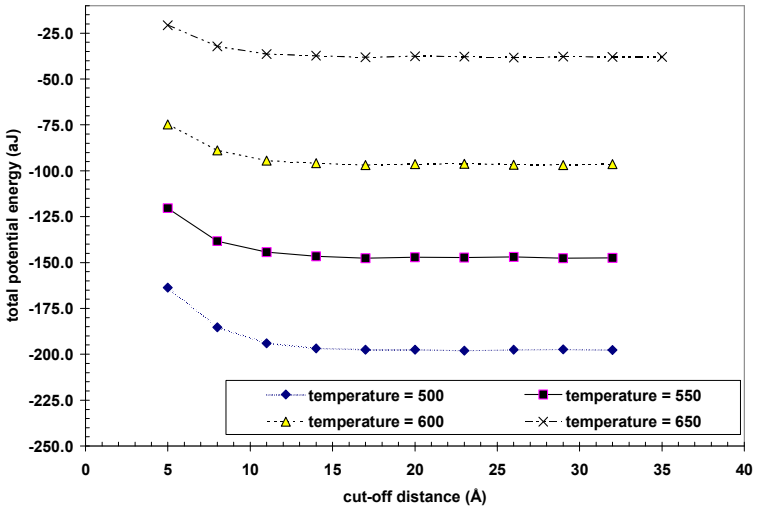

Figure 5.2: Total potential energy for different temperatures (Kelvin) in a two-phase simulation as functions of cut-off distance.

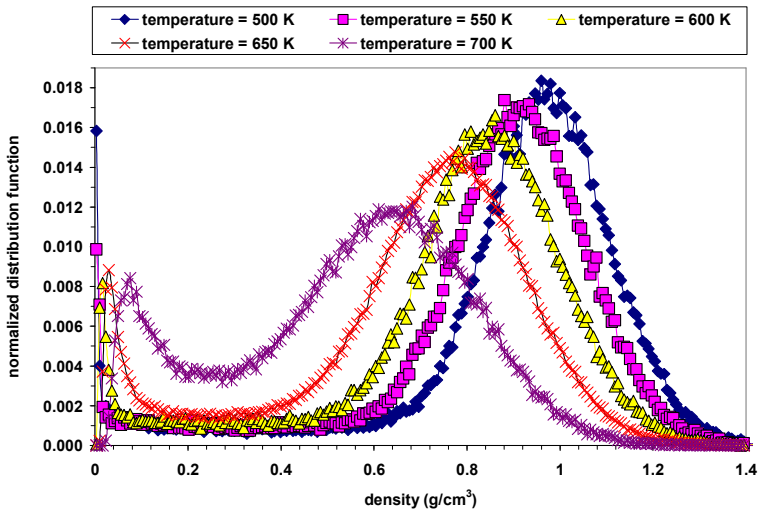

Figure 5.3: Two-phase density distributions of ethanediol as functions of temperature from Voronoi tessellations.

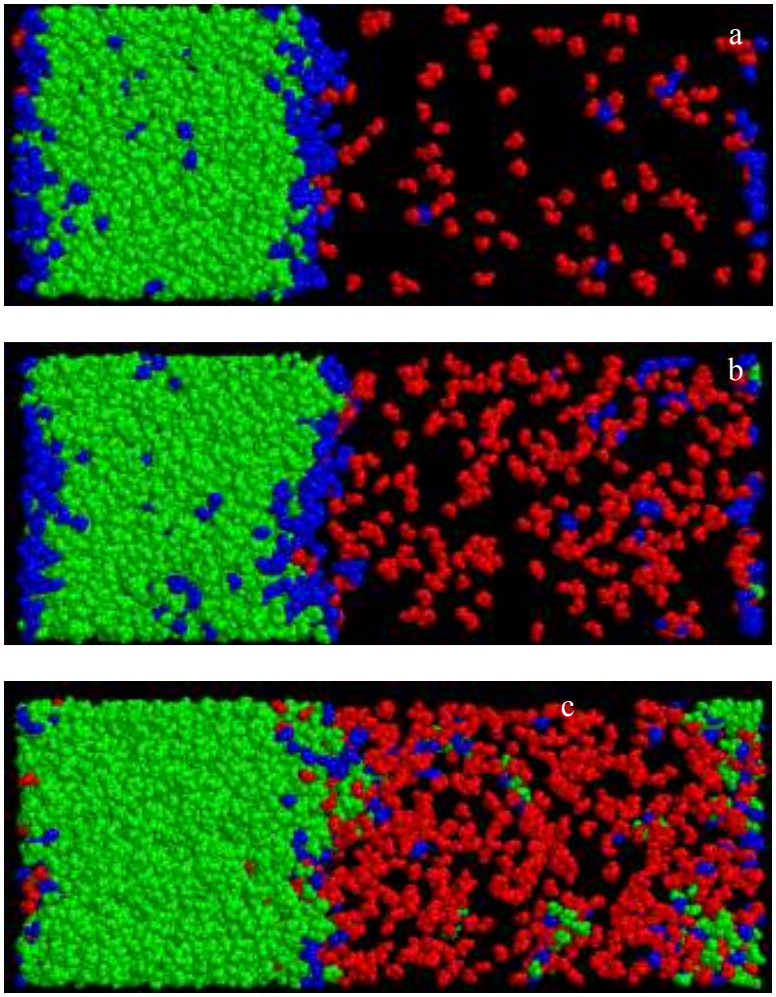

Figure 5.4: Snapshots of final configurations. The molecules are colored by their phase: green are liquid, red are vapor, and blue are interface (neither vapor nor liquid). (a) is 600 K, (b) is 650 K and (c) is 700 K.

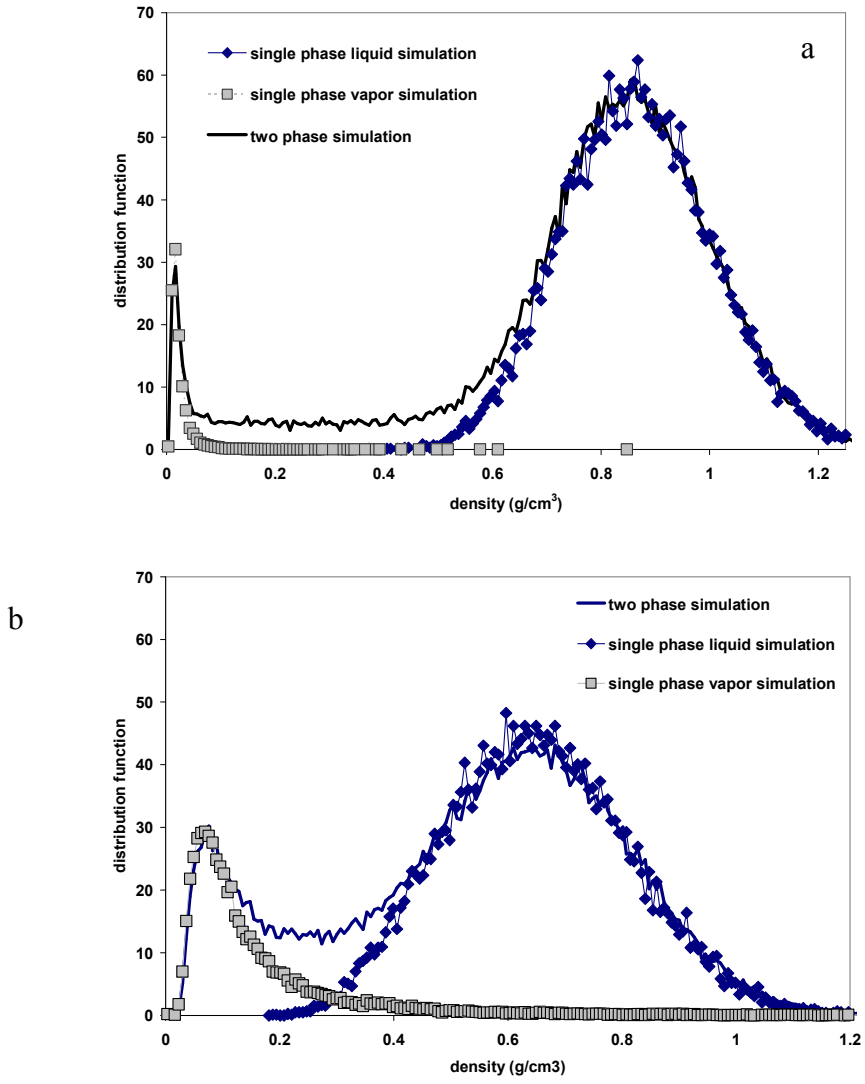

Figure 5.5: The unnormalized distribution functions for density. The blue boxes are the results from the single-phase liquid simulation, and the grey boxes are the results from the single-phase vapor simulation, and the solid line is the results from the two-phase simulation. (a) is 600 K and (b) is 700 K.

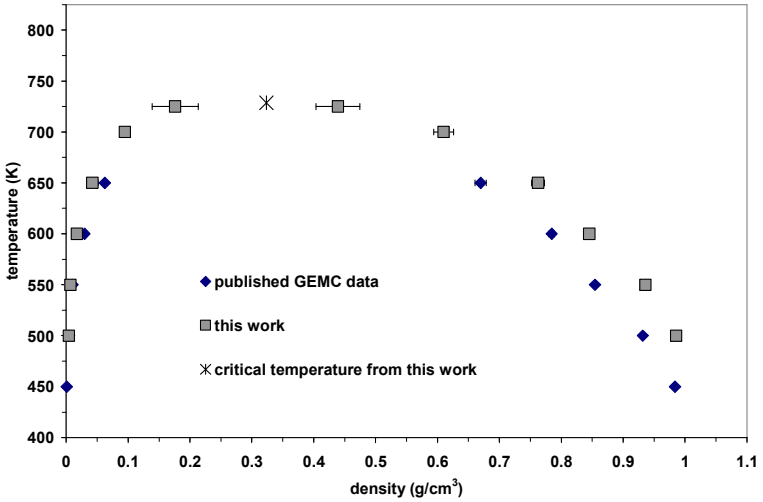

Figure 5.6: Phase diagram for ethanediol.

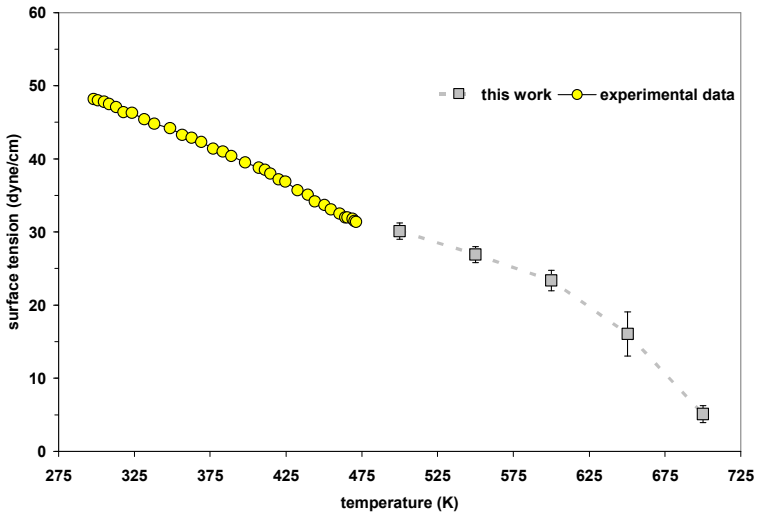

Figure 5.7: Surface tension of ethanediol.

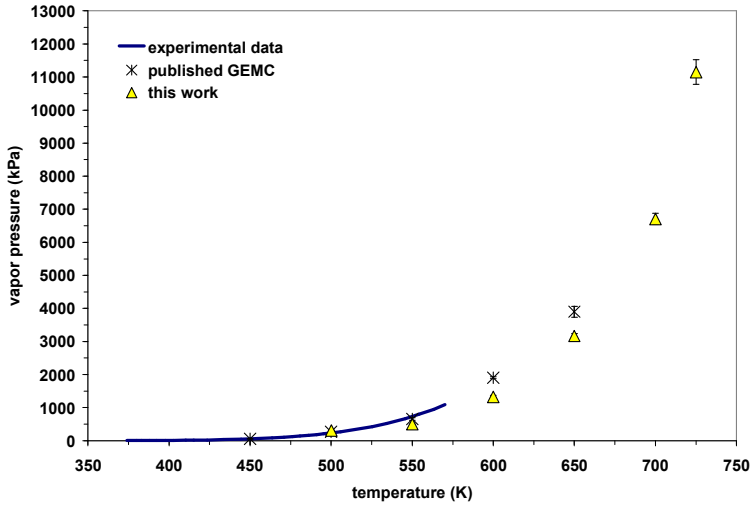

Figure 5.8: Vapor pressure of ethanediol.

Table5.3 Average properties determined for ethanediol.

T(K)	ρ_V (g/cm^3)	ρ_L (g/cm^3)	Pvap (kPa)	γ (dyn/cm)
500	0.0045	0.986	309.4	30.12
550	0.0070	0.936	497.9	26.91
600	0.0174	0.845	1323.9	23.37
650	0.0424	0.763	3163.9	16.07
700	0.0951	0.610	6707.1	5.10
T_c	728 (K)	ρ_C	0.338 (g/cm^3)	

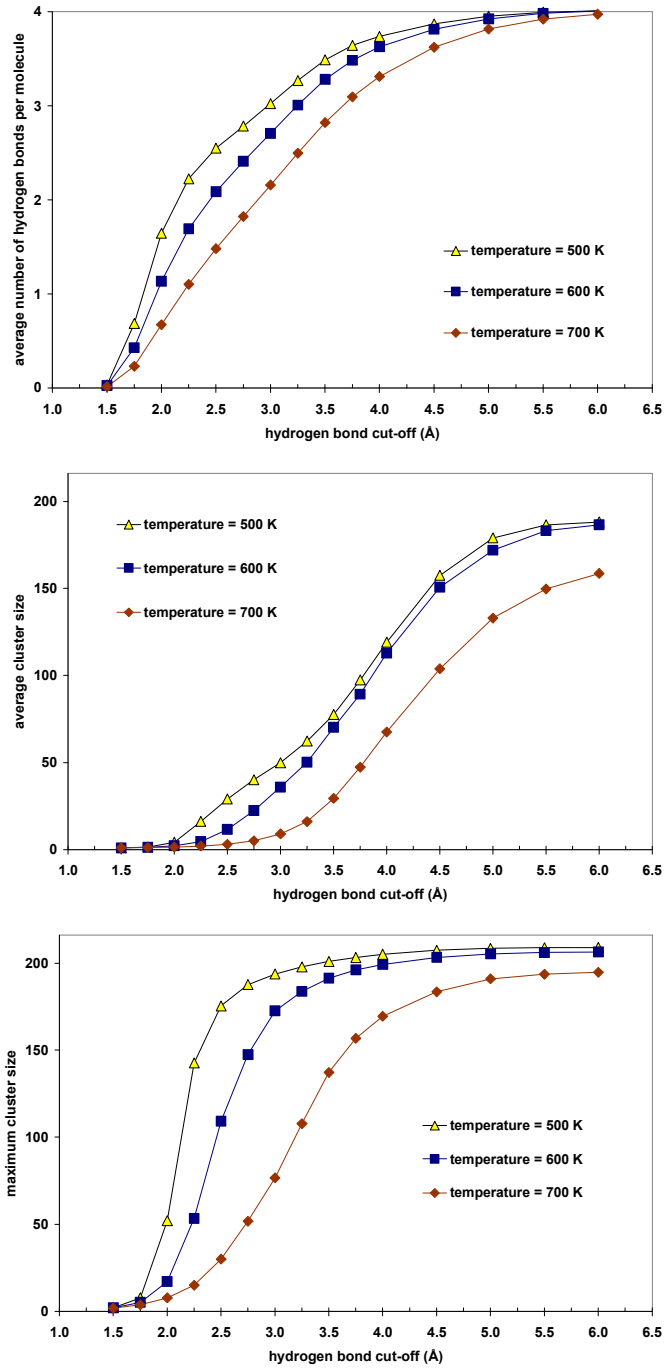

Figure 5.9: Hydrogen bonding for ethanediol. (a) is the average number of hydrogen bonds per molecule, (b) is the average cluster size, and (c) is the average maximum cluster size.

CHAPTER 6

Conclusions

6.1 Summary

The simulation of VLE by MD has been evolving since the mid 1970's and will continue to evolve into the future. History has provided us with good ideas for the extraction of the properties of individual phases. The earliest of these methods was to simply look at the density profile and fit it to functions to determine the average local properties of each phase. This method was considered the state of the art until 2000 when Gelb and Muller made the first attempt to determine truly local properties to define the phases. The fault in their work is that it required too many adjustable parameters. Chapter 2 exposed the problems with these methods. The adjustable parameters had to be "calibrated" at each temperature along the phase envelope to match the values from the equation of state. As such, this method worked well for a system where one already knows the answer and can tune the results to match the accepted value.

Although the method of Gelb and Muller did not work well for systems without known phase densities, the idea that local properties can lead to the extraction of bulk phase properties for a two-phase system was a great advancement in two-phase MD. Following the logic that the bulk phases can be defined by a local property, a method was presented in Chapter 3 that utilized Voronoi Tessellations to calculate the volume of every molecule in the simulation cell. The average value of the molecular volume is coupled to statistical parameters, such as the variance, to determine the individual phases. To insure self-consistency in the method the phase cut-offs were determined not from inspection of histograms but from single-phase simulations. When the normalized

variance from the single-phase simulation matches the normalized variance from the two-phase simulation the phase density is determined. This method allowed the phases to be in any configuration and no longer contiguous, and the local phenomena could be taken into account and not smeared into the bulk properties as with other methods. Chapter 3 also gave the first of three example systems for the phase determination. The example was a simple Lennard-Jones system, and the results were outstanding. The method was able to predict phase densities within 3% of the critical temperature. The method predicted at low temperatures that some molecules are considered vapor *or* liquid, at higher temperatures molecules can be considered both liquid *and* vapor. This changing definition of the interface is necessary because the phases break down as the temperature approaches the critical temperature giving way to local "pockets" of vapor and liquid.

Chapter 4 was the second of the three example systems investigated. The test case was ethanol. Explicit atom simulations of ethanol were carried out using the OPLS-AA force field. This was the first application of the Voronoi method to calculate the molecular volumes of a polyatomic system. It was necessary to determine if the calculation of the molecular volume could be determined from centers of mass of the molecule or if the volume of each atom had to be calculated and then summed into the molecular volume. The centers of mass resulted in the same volume as the summed volumes of the atoms. Much of the focus of Chapter 4 was upon the difficulty of implementation of the Voronoi Method in two-phase simulations. The difficulty arises from the starting simulation geometry. If the simulation cell geometry is chosen such that the box is very narrow in the x and y directions but is very long in the z axis, there are not

enough unique molecules for the tessellation to be performed correctly. Furthermore, there has to be enough molecules in the vapor phase to create the proper tessellation. These two constraints make it difficult to triangulate systems far from the critical temperature. Other properties investigated for ethanol in Chapter 4 are the phase densities, the critical properties, the vapor pressure, the molecular orientation at the interface, the surface tension, and the hydrogen bonding along the phase envelope.

The phase densities agree with published values from Gibbs Ensemble Monte Carlo (GEMC). Both the results from GEMC and this work are too low on the liquid side of the phase envelope and too high on the vapor side of the phase envelope, as compared to the experimental data for ethanol. The vapor pressure and the surface tension are always higher than the expected experimental values. Hydrogen bonding along the phase envelope was investigated by determining the oxygen-hydrogen pair correlation functions. There is substantial hydrogen bonding between the hydroxyl hydrogen and the oxygen on different molecules in both the liquid and vapor phases. The hydroxyl hydrogen does not readily hydrogen bond with the methyl group.

The final example system investigated in this study was ethanediol. Ethanediol was simulated utilizing the Transferable Potentials for Phase Equilibria (TraPPE), and is represented by united atoms. The united atom representation of ethanediol removes the hydrogens bound to the carbon atoms, but the hydroxyl hydrogens are represented explicitly. In order to determine accurately the vapor pressure and the surface tension of ethanediol the bond stretching parameters had to be fit. To do this, Gaussian 98 was used

to scan the potential energy surface for various bond lengths, the calculations were performed at the B3LYP/6-31G* level.

The phase envelope was determined by using the Voronoi Method on the center of mass of each molecule. There is a difference between our values for the vapor and liquid densities and those published in the literature. This discrepancy can be attributed to the flexible bonds that were incorporated because the effect of changing the bond lengths without regard to the other potential parameters may have caused the density along the phase envelope to change.

Other properties investigated in Chapter 5 are the critical properties, the surface tension, the vapor pressure, and hydrogen bonding along the phase envelope.

6.2 The Bigger Picture

There are many new features introduced in this work that were important to the simulation of VLE. The bulk phase densities were determined utilizing a local property and order parameter. All of the ambiguity and adjustable parameters were removed from the determination of the phases. The removal of this ambiguity resulted in a self-consistent method to determine the phases of any system without *a priori* knowledge of the phase density which is important for the investigation of unknown compounds.

Because of the new method created, sampling of higher temperatures along the phase envelope can be performed. This sampling allows for the investigation of a region previously thought off limits, the near critical region. The investigation of a near critical

fluid was briefly investigated in Chapter 3 and 4. Near the critical point, the bulk phases are no longer contiguous; the bulk phases begin to break down into smaller individual regions of vapor and liquid. This could not be accounted for in any other method to date.

One novel concept that has emerged from this work is the nature of molecules in the interface. At low temperatures, it is found that the interface is made up of molecules that are "neither vapor nor liquid". In other words, these interfacial molecules have Voronoi volumes in the two-phase simulation that are not present in either the pure liquid or pure vapor simulations. At high temperatures, it is found that the interface is composed of molecules that are "both vapor and liquid". In other words, these interfacial molecules have Voronoi volumes that are present in both the pure liquid and pure vapor simulations.

The distribution of interfacial molecules is also interesting. Using this Voronoi method, we find "interfacial molecules" to be concentrated at the interface of the liquid and vapor phases. However, we also find some "interfacial particles" scattered through the bulk phases. This leads us to the following concept. In a single-phase system, the Voronoi volume of a given particle fluctuates around the mean molecular volume. At times these fluctuations take the molecule into regions of either unusually high or unusually low volumes. In a single-phase system, a molecule with these types of volumes is unstable. Although the current understanding of thermodynamics does not allow us to define a free energy of an individual molecule, clearly such a concept is needed here to provide the thermodynamic driving force to return a molecule with a wide volume fluctuation back to the mean volume.

In a two-phase system, the presence of the macroscopic inhomogeneity in density that is the most obvious characteristic of the vapor/liquid interface stabilizes volume fluctuations at values far from the mean of either the vapor or the liquid. The ability of a macroscopic inhomogeneity in density to stabilize an otherwise unstable local fluctuation is very interesting.

The application of this method to polyatomic systems proves that Molecular Dynamics is as reliable and accurate as any Monte Carlo method for the study of VLE. In fact, many of the Monte Carlo methods break down close to the critical point, where the method here can sample any system with multiple phases. Therefore, the phase densities, the surface tension, and the molecular orientation can all be determined from one single simulation.

At this point, a method has been developed for the determination of VLE data via two-phase MD simulation that is self-consistent and can be applied to simple or polyatomic molecules. Importantly, in this method we have eliminated any arbitrary choices used to distinguish phases. As always, the accuracy of the results is dependent upon the degree to which the interaction potential correctly models the interactions in the real system.

6.3 Future Work

There are still many avenues for new interesting research for the Voronoi Method applied to phase equilibria. The simulation of a multicomponent multiphase system has

never been accomplished and could be performed with the same procedure created in Chapter 3. The volumes of each component would need to be calculated and separated. Single-phase simulations of each component could then be performed to determine the phase cut-offs. This method could be developed by utilizing a simple Lennard-Jones system.

In addition to multicomponent systems, other phase equilibrium points could be investigated. One example would be the triple point. This system could also be a simple fluid and the three-phase system would need to be simulated, followed by single-phase simulations in each phase. Modifications might need to be made to the Voronoi Method to account for the dilute phase. This modification may be splitting the triangulation into different regions for the dense and dilute phases and then recombining.

One admitted limitation of the Voronoi Method is the fact that we have chosen to match the distribution of the Voronoi volume in the two-phase and one-phase simulations based exclusively on the mean and variance. It does not guarantee the same shape of the distribution beyond these two characteristics. One refinement to the Voronoi Method would be to account for higher moments in the statistical analysis of the phases. The need for higher moments may become necessary as the temperature approaches the critical temperature because the single-phase distributions in systems with hydrogen bonding become highly skewed at higher temperatures. Consequently, although we have matched the mean and variance of the distribution of the Voronoi volume in the two-phase and one-phase simulations, the shapes of the distributions are not identical.

Finally, there currently exists no theory that can predict the distribution of Voronoi volumes even in the single-phase system. Such a theory would be useful to this procedure, since it would allow us to match the shape of distributions and not just the mean and variance. This theory requires an understanding of the free energy of individual molecules as functions of their Voronoi volumes. This understanding does not currently exist, even for the ideal gas. Theoretical research in this direction would be useful and could potentially be applied to understanding the stability of individual molecules in a variety of systems with nanoscale structure.

References

(1) van der Waals, J. D. On the continuity of the gaseous and liquid states; Elsevier Science Publications: Amsterdam; New York: North-Holland; New York, N.Y., U.S.A., 1988.

(2) Niktin, E. D.; Palov, P. A.; Scripov, P. V. J. Chem. Thermodyn **1993**, 25, 869.

(3) Steele, W. V.; Chirco, R. D.; Cowell, A. B.; Knipmeyer, S. E.; Nguyen, A. J. Chem. Eng. Data **2002**, 47, 667.

(4) http://webbook.nist.gov/

(5) Allen, M. P.; Tildesley, D. J. Computer Simulation of Liquids; Clarendon Press: Oxford, 1989.

(6) Frenkel, D.; Smit, B. Understanding Molecular Simulation From Algorithms to Applications, Second Edition ed.; Academic Press: San Diego, Ca, 2002.

(7) Chapela, G. A.; Saville, G.; Thompson, S. M.; Rowlinson, J. S. J. Chem. Soc., Faraday Trans. **1977**, 73, 1133.

(8) Ladd, A. J. C.; Woodcock, L. V. Mol. Phys. **1978**, 36, 611.

(9) Panagiotopoulos, A. Z. J. Phys.:Condens. Matter **2000**, 12, R25.

(10) Gelb, L. D.; Müller, E. A. Fluid Phase Equilib. **2002**, 203, 1.

(11) Martinez-Veracoechea, F.; Müller, E. A. Mol. Simul. **2005**, 31, 33.

(12) Pamies, J. C.; McCabe, C.; Cummings, P. T.; Vega, L. F. Mol. Simul. **2003**, 29, 463.

(13) Fern, J. T.; Keffer, D. J.; Steele, W. V. J. Phys. Chem. B **2007**, 111, 3469.

(14) Aurenhammer, F. ACM Computing Surveys **1991**, 23, 345.

(15) Gerstein, M.; Tsai, J.; Levitt, M. J. Mol. Biol. **1995**, 249, 955.

(16) O'Rourke, J. Computational Geometry in C; Cambridge University Press: New York, 1994.

(17) Fern, J. T.; Keffer, D. J.; Steele, W. V. J. Phys. Chem. B **accepted for publication**.

(18) Jorgensen, W. L.; Maxwell, D. S.; TiradoRives, J. J. Am. Chem. Soc. **1996**, 118, 11225.

(19) Wolf, D.; Keblinski, P.; Phillpot, S. R.; Eggebrecht, J. J. Chem. Phys. **1999**, 110, 8254.

(20) Martin, M. G. Fluid Phase Equilib. **2006**, 248, 50.

(21) Frisch, M. J. T., G. W.; Schlegel, H. B.; Scuseria, G. E. R., M. A.; Cheeseman, J. R.; Zakrzewski, V. G.; Montgomery, J. A.; Stratmann, R. E. B., J. C.; Dapprich, S.; Millam, J. M.; Daniels, A. D.; Kudin, K. N.; Strain, M. C. F., O.; Tomasi, J.; Barone, V.; Cossi, M.; Cammi, R.; Mennucci, B.; Pomelli, C. A., C.; Clifford, S.; Ochterski, J.; Petersson, G. A.; Ayala, P. Y.; Cui, Q.; Morokuma, K. M., D. K.; Rabuck, A. D.; Raghavachari, K.; Foresman, J. B.; Cioslowski; J.; Ortiz, J. V. S., B. B.; Liu, G.; Liashenko, A.; Piskorz, P.; Komaromi, I.; Gomperts; R.; Martin, R. L. F., D. J.; Keith, T.; Al-Laham, M. A.; Peng, C. Y.; Nanayakkara, A.; Gonzalez, C. C., M.; Gill, P. M. W.; Johnson, B. G.; Chen, W.; Wong, M. W.; Andres, J. L. H.-G., M.; Replogle E. S.; Pople, J. A. **1998**.

(22) McCabe, C. Ind. Eng. Chem. Res **2004**, 43, 2839.

(23) Johnson, J. K.; Zollweg, J. A.; Gubbins, K. E. Mol. Phys. **1993**, 78, 591.

(24) *Majer, V.; Svoboda, V. Enthalpies of Vaporization of Organic Compunds: A Critical Review and Data Compilation; Blackwell Scientific Publications: Oxford, 1985.*
(25) *Setzmann, U.; Wagner, W. J. Phys. Chem. Ref. Data* ***1991****, 20, 1061.*
(26) *Hoover, W. G. Phys. Rev. A* ***1985****, 31.*
(27) *Nose', S. J. Chem. Phys* ***1984****, 81, 511.*
(28) *Gear, C. W. The Numerical Integration of Ordinary Differential Equations of Various Orders; Argonne National Laboratory, 1966.*
(29) *Gear, C. W. Numerical Initial Value Problems in Ordinary Differential Equations; Prentice Hall, Inc.: Englewood Cliffs, New Jersey, 1971.*
(30) *Bird, B. R.; Stewart, W. E.; Lightfoot, E. N. Transport Phenomena; John Wiley & Sons, Inc.: New York, 2002.*
(31) *Holcomb, C. D.; Clancy, P.; Thompson, S. M.; Zollweg, J. A. Fluid Phase Equilibria* ***1993****, 88, 303.*
(32) *Trokhymchuk, A.; Alejandre, J. Journal of Chemical Physics* ***1999****, 111, 8510.*
(33) *Duque, D.; Vega, L. F. J. Chem. Phys.* ***2004****, 121, 8611.*
(34) *Rowlinson, J. S. Liquids and Liquid Mixtures; Butterworth & Co: London, 1969.*
(35) *Rowlinson, J. S.; Windom, B. Molecular Theory of Capillarity; Oxford University Press: New York, 1982.*
(36) *Holcomb, C. D.; Clancy, P.; Thompson, S. M.; Zollweg, J. A. Fluid Phase Equilib.* ***1992****, 75, 185.*
(37) *Lofti, A.; Vrabec, J.; Fischer, J. Molecular Physics* ***1992****, 76, 1319.*
(38) *Windom, B. J. Chem. Phys* ***1963****, 39, 2808.*
(39) *Pe'rez-Pellitero, J.; Ungerer, P.; Orkoulas, G.; Mackie, A. D. The Journal of Chemical Physics* ***2006****, 125, 054515.*
(40) *Pontoff, J. J.; Panagiotopoulos, A. Z. Journal of Chemical Physics* ***1998****, 109, 10914.*
(41) *Duyckaerts, C.; Godefroy, G. Journal of Chemical Neuroanatomy* ***2000****, 20, 83.*
(42) *Kumar, V. S.; Kumaran, V. J. Chem. Phys.* ***2005****, 123, 074502.*
(43) *Kumar, V. S.; Kumaran, V. J. Chem. Phys.* ***2005****, 123, 114501.*
(44) *Alejandre, J.; Tildesley, D.; Chapela, G. Molecular Physics* ***1995****, 85, 651.*
(45) *Trokhymchuk, A.; Alejandre, J. Journal of Chemical Physics* ***1999****, 111, 8510.*
(46) *Nose', S. Mol. Phys.* ***1984****, 52.*
(47) *McQuarrie, D. A. Statistical Mechanics; University Science Books: Sausalito Ca, 2000.*
(48) *Kofke, D. A. Mol. Phys.* ***1993****, 78, 1331.*
(49) *Kofke, D. A. J. Chem. Phys.* ***1993****, 98, 4149.*
(50) *Vrabec, J.; Kedia, G. K.; Fuchs, G.; Hasse, H. Mol. Phys.* ***2006****, 104, 1509.*
(51) *Taylor, R. S.; Shields, R. L. J. Chem. Phys.* ***2003****, 119, 12569.*
(52) *Xiong, R.; Fern, J. T.; Kassaee, M. H.; Chen, Y.; Steele, W. V.; Zhang, X. P.; Keffer, D. J. J. Phys. Chem. C, under review.*
(53) *Dillon, H. E.; Penoncello, S. G. Int. J. Thermophys.* ***2004****, 25, 321.*
(54) *Martyna, G. J.; Tuckerman, M. E.; Tobias, D. J.; Klein, M. L. Mol. Phys.* ***1996****, 87, 1117.*

(55) *Tuckerman, M. E.; Berne, B. J.; Martyna, G. J. J. Chem. Phys* ***1992****, 97, 1990.*
(56) *Irving, J. H.; Kirkwood, J. G. J. Chem. Phys.* ***1950****, 18, 817.*
(57) *Kirkwood, J. G.; Bluff, F. P. J. Chem. Phys.* ***1949****, 17, 338.*
(58) *Nicolas, J. P.; Souza, N. R. d. J. Chem. Phys.* ***2004****, 120, 2464.*
(59) *Guo, M.; Lu, B. C.-Y. J. Chem. Phys.* ***1996****, 106, 3688.*
(60) *Blokhuis, E. M.; Bedeaux, D.; Holcomb, C. D.; Zollweg, J. A. Mol. Phys.* ***1995****, 85, 655.*
(61) *Yaws, C. L. Chemical Properties HandbookNew York, NY, 1999.*
(62) *Curtiss, L. A.; Blander, M. Chem. Rev.* ***1988****, 88, 827.*
(63) *Hoffmann, M. M.; Conradi, M. S. J. Phys. Chem. B* ***1997****, 102, 263.*
(64) *Patel, S.; III, C. L. B. J. Chem. Phys.* ***2005****, 123, 1.*
(65) *González, L.; Mó, O.; Yáñez, M. J. Chem. Phys.* ***1999****, 111, 3855.*
(66) *Ambrose, D.; Sprake, C. H. S. J. Chem. Thermodyn.* ***1970****, 2, 631.*
(67) *www.nist.gov*
(68) *Nikitin, E. D.; Palov, P. A.; Scripov, P. V. J. Chem. Thermodyn* ***1993****, 25, 869.*
(69) *Stubbs, J. M.; Pontoff, J. J.; Siepmann, J. I. J. Phys. Chem. B* ***2004****, 108, 17596.*
(70) *Vrabec, J.; Hasse, H. Mol. Phys.* ***2002****, 100, 3375.*
(71) *Duque, D.; Pamies, J. C.; Vega, L. F. Journal of Chemical Physics* ***2004****, 121, 11395.*
(72) *Kassaee, M. H.; Keffer, D. J.; Steele, W. V. J. Chem. Eng. Data* ***2007****, 52, 1843.*
(73) *Kassaee, M. H.; Keffer, D. J.; Steele, W. V. Theochem* ***2007****, 802, 23.*
(74) *Hoke, B. C.; Chen, J. C. J. Chem. Eng. Data* ***1991****, 36, 322.*
(75) *Jasper, J. J. J. Phys. Chem. Ref. Data* ***1972****, 1, 841.*

VITA

Jared Thomas Fern was born in Royal Oak, Michigan in December of 1979. He was raised in by his parents Thomas and Gail Fern. In 1992, Thomas was asked to transfer from his job in Michigan to a position in Tennessee. Jared went to elementary school at Brown School and Woodard Elementary schools in Columbia, Tennessee. After elementary school he attended Whitthorne Middle School followed by Columbia Academy for high school.

In 1998, Jared graduated from high school and attended Middle Tennessee State University in Murfreesboro, Tennessee. At MTSU, he majored in Chemistry and Biology. After two years at MTSU, Jared transferred to the University of Tennessee, Knoxville. At UTK he majored in Chemical Engineering with a minor in Chemistry, and his primary advisor was Dr. John Prados. In the spring of 2003, he graduated with his Bachelors degree in Chemical Engineering.

In the fall of 2003, Jared entered graduate school at UTK. He majored in Chemical Engineering, and was advised by Dr. David Keffer and Dr. William Steele. In the spring of 2006, the department of Chemical Engineering awarded him the Jim and Sandra McKinley Outstanding Graduate Student Award.

Jared graduated with a PhD in Chemical Engineering from the University of Tennessee, Knoxville in December of 2007.